NASA TECHNICAL REPORT

NASA TR R-303

NASA TR R-303

CAUSES OF MAGNETIC-FIELD NONUNIFORMITY AND ITS EFFECT ON STABILITY OF THETA-PINCH PLASMA

by Joseph Norwood, Jr.

Langley Research Center
Langley Station, Hampton, Va.

NATIONAL AERONAUTICS AND SPACE ADMINISTRATION • WASHINGTON, D. C. • MARCH 1969

NASA TR R-303

CAUSES OF MAGNETIC-FIELD NONUNIFORMITY AND ITS EFFECT ON STABILITY OF THETA-PINCH PLASMA

By Joseph Norwood, Jr.

Langley Research Center
Langley Station, Hampton, Va.

NATIONAL AERONAUTICS AND SPACE ADMINISTRATION

For sale by the Clearinghouse for Federal Scientific and Technical Information
Springfield, Virginia 22151 – CFSTI price $3.00

CONTENTS

CAUSES OF MAGNETIC-FIELD NONUNIFORMITY AND ITS EFFECT ON STABILITY OF THETA-PINCH PLASMA*

By Joseph Norwood, Jr.
Langley Research Center

SUMMARY

The various instabilities which beset the theta-pinch plasma are described in some detail, and the importance of the role of magnetic-field uniformity is demonstrated. Sources of the field nonuniformity are delineated and discussed. These include the collector-plate geometry, the nonlinear effect of the plasma, end effects in the coil, discontinuity in gap spacing as the current flows into the coil, and effects of the alteration in axial current distribution due to skin effect.

Next the various methods for stabilizing the plasma by eliminating field gradients are described, and a new method involving the use of a flux concentrator is proposed. The advantages of this method are compared with advantages of other techniques that have been used. Also, results of quantitative measurements of the field uniformity in an exact 1/2-scale model of the Langley theta pinch are presented. These results include flux-concentrator and collector-plate-extension effects as well as the effect of the volume of the collector-plate structure which excludes high-frequency flux due to skin effect. Finally, experiments which suggest that full-scale theta pinches without extensions are capable of being stabilized by flux-concentrator techniques are described.

INTRODUCTION

The central problem in the confinement and heating of high-temperature plasmas is the production of a stable equilibrium, or, more realistically, the elimination or suppression of those instabilities whose growth time is less than the attempted time of confinement. The theta-pinch geometry, in which a plasma column is confined and compressed by an axial magnetic field that is sinusoidal in time, has attracted considerable attention, and work on this configuration has been pursued at various laboratories throughout the world (ref. 1). The most dangerous of the instabilities which beset the theta-pinch plasma

*The information presented herein was included in a dissertation entitled "Stabilization of Plasma in a Theta Pinch" offered in partial fulfillment of the requirements for the degree of Doctor of Philosopy in Physics, Stevens Institute of Technology, Hoboken, New Jersey, 1967.

have been shown to be caused by deviations from uniformity of the magnetic field (ref. 2) and by finite resistivity effects (ref. 3). The purpose of this paper is to point out the various causes of field nonuniformity in a theta pinch and to discuss the effect of such nonuniformity on the stability. Quantitative measurements of the uniformity of the vacuum magnetic field in a 1/2-scale model of the Langley magnetic compression experiment (i.e., in a 1/2-scale model of the Langley theta pinch) are made for various conductor geometries. The effect of a flux concentrator on the field uniformity is compared with the effect of a collector-plate extension and the presence or absence of part of the flux-excluding volume of the collector-plate structure. Tests on the full-scale Langley theta pinch which demonstrate reduction of the drift velocity through the use of prototype flux concentrators are described. Probe measurements on a 1/5-scale model of the Naval Research Laboratory (NRL) theta pinch (ref. 4) were made for a restricted case with much less accuracy than was obtained in the present investigation.

SYMBOLS

A	area of hole through which particle losses occur, meters^2
a	radius of coil in conformal mapping, meters
B	magnetic flux density, teslas
b	width of transmission line, meters
c	speed of light, meters/second
c_v	specific heat per unit volume, joules/kilogram-meters^3
d	extension gap spacing, meters
E	electric-field strength, volts/meter
e	electronic charge (with power indicated by superscript u or w), coulombs
F	force, newtons
g	acceleration of plasma, meters/second^2; acceleration of gravity, 9.8 meters/second^2

$g(x,y)$	spatial function of x and y
h	gap spacing of transmission line, meters
I	electrical current, amperes
j	electrical current density, amperes/meter^2
j_z	axial Hall current density, amperes/meter^2
j_θ	azimuthal current density, amperes/meter^2
k	wave number, meter^{-1}
L	inductance, henries
ℓ	extension length, meters
M	plasma mass per unit axial length, kilograms/meter
m	mode number
m_i	ion mass, kilograms
N	number of particles
n	particle density, meter^{-3}
q	charge, coulombs
R	radius of curvature of field lines, meters
r	radial distance from coil axis, meters
r_1	inner radius of plasma column, meters
r_2	outer radius of plasma column, meters
T	temperature, degrees Kelvin

t	time, seconds; thickness of coil wall, meters
$U = \Omega/k$	
u	real part of complex variable w
v	imaginary part of complex variable w
v_{th}	thermal ion velocity, meters/second
$v_{\parallel}$	ion velocity parallel to $\vec{B}$, meters/second
$v_{\perp}$	ion velocity perpendicular to $\vec{B}$, meters/second
v_{θ}	rotational velocity, meters/second
$\bar{v}$	mean ion velocity, meters/second
$\bar{v}_{th}$	mean thermal ion velocity, meters/second
w	complex variable; drift velocity, meters/second; extension width, meters
w^E	zero-order drift, meters/second
X	radius of curvature of coil end, meters
x	real part of complex variable z
y	imaginary part of complex variable z
Z	coil axis; nuclear charge
z	complex variable; axial distance from the coil center, meters
α	probe discrimination coefficient
β	ratio of kinetic energy density to sum of magnetic and kinetic energy densities
δ	thickness of plasma boundary layer, meters; skin depth, meters

ϵ_o	vacuum permittivity, farads/meter
θ	incremental angle, radians
κ	Boltzmann constant, 1.3805×10^{-23} joule/degree Kelvin
μ_m	magnetic moment per unit length of plasma column, amperes/meter
μ_o	vacuum permeability, henries/meter
ρ	mass density, kilograms/meter^3
σ	electrical conductivity, reciprocal ohms/meter
τ	plasma implosion time, seconds; acceleration time constant; duration of current pulse, seconds
Ω	ion cyclotron frequency, second^{-1}
ω	angular frequency of coil current
ω_g	reciprocal of instability growth time, second^{-1}

Subscripts:

max	maximum
o	compression field
r	radial component
T	trapped field
z	z-component
τ	at time of plasma implosion
∞	at $r = 0$ and $x = \infty$

Dots over symbols indicate derivatives with respect to time; arrows over symbols indicate vectors.

INSTABILITIES OF THETA PINCH

Drift Instability

In many theta-pinch experiments the plasma column is observed to drift transversely in the plane of the collector plates either toward, as is usually the case, or away from the slot. The force $\vec{F}$ is due to interaction between the magnetic moment of the plasma column $\vec{\mu}_m$, which is assumed to have only a z-component, and gradients of the confining magnetic field $\vec{B}_o$, as indicated in the following equation:

$$\vec{F} = -\left(\vec{\mu}_m \cdot \nabla\right)\vec{B}_o \tag{1}$$

The magnetic field in the coil (see fig. 1) is taken to be

$$\left.\begin{aligned} B_z &= B_T && \left(r < r_1\right) \\ B_z &= \frac{B_o\left(r - r_1\right) - B_T\left(r - r_2\right)}{r_2 - r_1} && \left(r_1 < r < r_2\right) \\ B_z &= B_o && \left(r > r_2\right) \end{aligned}\right\} \tag{2}$$

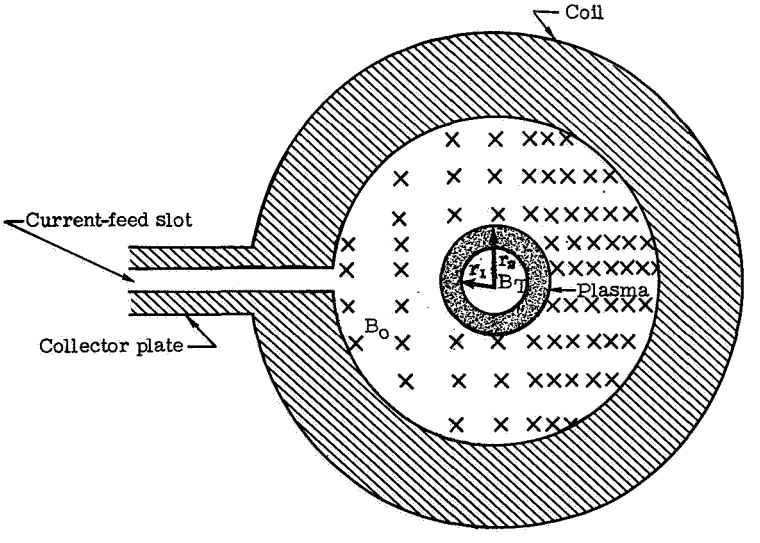

Figure 1.- Magnetic-field model for drift calculation.

where B_T, the trapped magnetic field, may be either positive or negative. From equation (1), $F_r = \mu_m \frac{\partial B_{o,r}}{\partial z}$; however, since the field in the coil for $r > r_2$ is due only to currents in the external conductors, the curl of B_o vanishes and $\partial B_{o,r}/\partial z$ may be replaced by $\partial B_{o,z}/\partial r$. The transverse acceleration of the plasma column may then be written as

$$\ddot{r} = -\frac{\mu_m \frac{dB_{o,z}}{dr}}{M}$$

where μ_m is the magnetic moment per unit length of the column and M is the plasma mass per unit axial length. The magnetic moment per unit length is given by

$$\mu_m = \int_{r_1}^{r_2} j\pi r^2 dr \tag{3}$$

Using Ampere's law for the current density

$$j = \frac{1}{\mu_o}\frac{dB_z}{dr} \qquad (r < r_2)$$

and equation (2), one finds

$$\mu_m = \frac{\pi(B_o - B_T)}{\mu_o(r_2 - r_1)}\frac{r_2^3 - r_1^3}{3} \tag{4}$$

Thus the transverse acceleration of the plasma column becomes

$$\ddot{r} = -\frac{\pi}{3}\frac{B_o - B_T}{\mu_o M}\frac{dB_{o,z}}{dr}\frac{r_2^3 - r_1^3}{r_2 - r_1} \tag{5}$$

With

$$\frac{1}{B_o}\frac{dB_{o,z}}{dr} = -\frac{1}{R}$$

where R is the radius of curvature of the field lines and where $B_o = B_{max} \sin \omega(t + \tau)$ (with B_{max} being the peak magnetic flux density, ω the angular frequency of the coil current, and τ the plasma implosion time), equation (5) integrates to

$$r = \frac{\pi B_{max}^2}{3\mu_o MR}\frac{r_2^3 - r_1^3}{r_2 - r_1}\left(\frac{1}{2\omega}\left\{\frac{1}{4\omega}\left[\cos 2\omega(t + \tau) - \cos 4\omega\tau\right] + \frac{\omega}{2}(t - \tau)(t + 3\tau)\right.\right.$$

$$\left.\left. + \frac{t - \tau}{2}\sin 4\omega\tau\right\} + \frac{B_T}{\omega B_{max}}\left\{\frac{1}{\omega}\left[\sin \omega(t + \tau) - \sin 2\omega\tau\right] - (t - \tau)\cos 2\omega\tau\right\}\right) \qquad (6)$$

This equation is derived with the assumption that the linear mass density M and radius of curvature of the field lines R are constant. Considering the plasma implosion time τ to be negligibly small and letting B_T be zero with r_1 consequently going to zero, one finds

$$r \approx \frac{B_{max}^2}{6\mu_o n m_i R\omega}\left[\frac{1}{4\omega}(\cos 2\omega t - 1) + \frac{\omega t^2}{2}\right] \qquad (7)$$

By taking values of B_{max}, n, m_i, and ω appropriate to the Langley theta pinch and using a value for R measured in the Naval Research Laboratory experiment (ref. 4), which is geometrically similar, the curve shown in figure 2 is plotted from equation (7). The constancy of R and n is confirmed by plotting the measured displacement of the plasma column as a function of $\frac{1}{4\omega}(\cos 2\omega t - 1) + \frac{\omega t^2}{2}$ and comparing the results with a straight line. This constancy is verified by the moderate point scatter shown in figure 2. The measured points were taken by streak photography with a rotating-mirror camera looking at the plasma in the median plane of the coil from the bottom – that is, recording plasma motion in the horizontal plane. The streak photograph is shown in figure 3. This shot was made with a main-capacitor-bank energy of 335 kilojoules and a filling pressure of 100 millitorr (13.3 N/m^2) of hydrogen. No bias magnetic field was employed, but because bias fields are often used, the trapped magnetic field B_T representing a bias field is included in the theory.

The agreement between theory and experiment is not as good at higher energies, as can be seen in figure 4, which was plotted from measurements of the streak photograph shown in figure 5. This shot was made with a filling pressure of 13.3 N/m^2 of hydrogen, no bias field, and an energy of the main capacitor bank of 1 megajoule. The lesser agreement stems from the fact that the particle density n and the radius of curvature of the field lines R were assumed to be constant. The assumption of a constant particle density is certainly poor at high energies since, without magnetic mirrors or a reversed

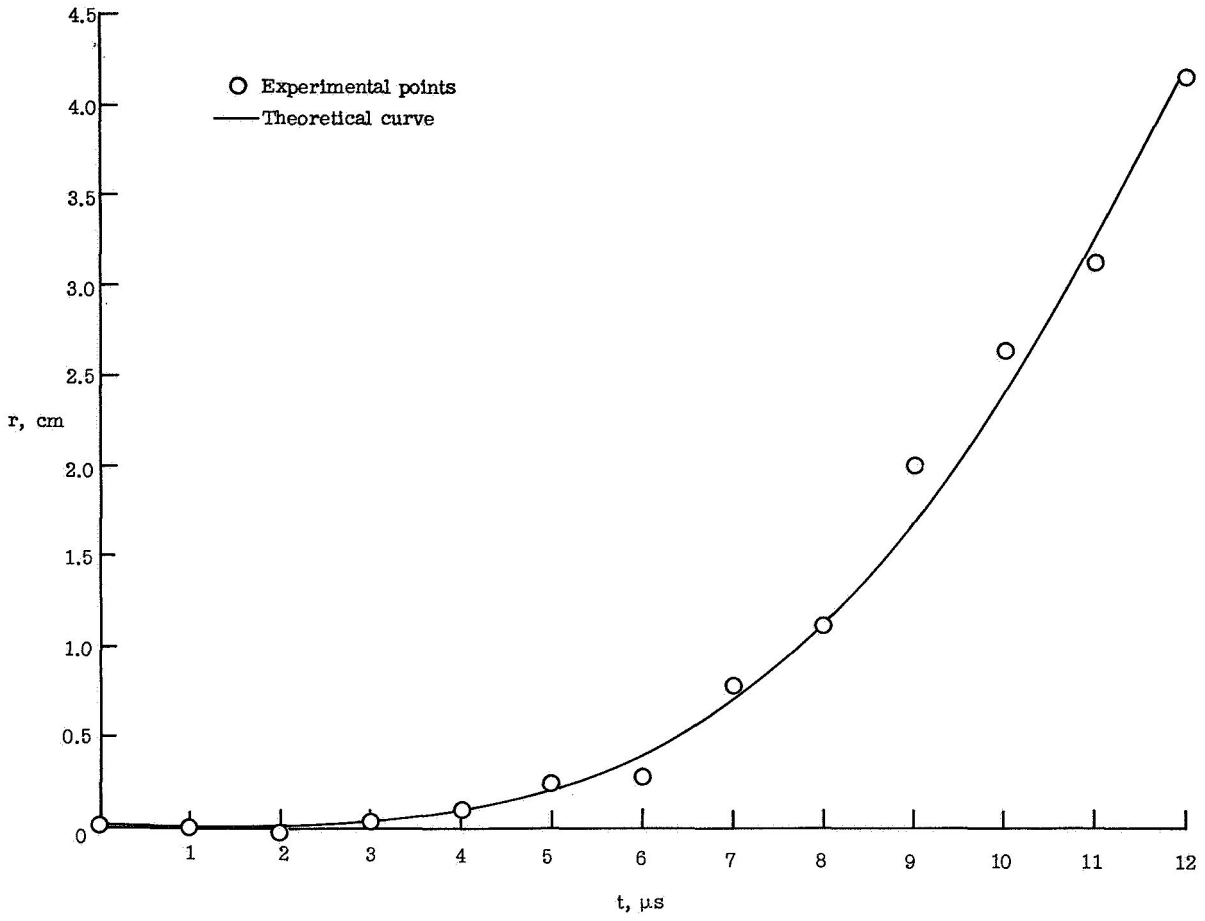

Figure 2.- Plasma drift in the Langley theta pinch with a capacitor-bank energy of 335 kilojoules.

Figure 3.- Streak photograph of drift plotted in figure 2. L-68-10,074

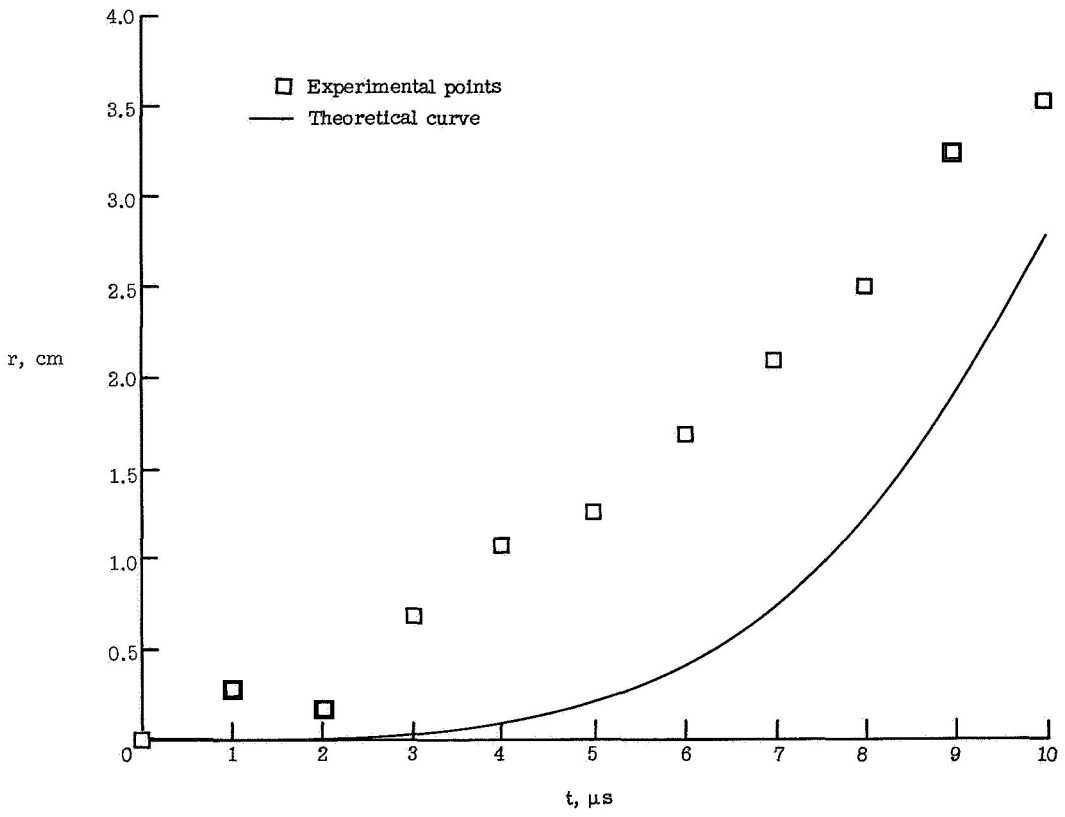

Figure 4.- Plasma drift in the Langley theta pinch with a capacitor-bank energy of 1 megajoule.

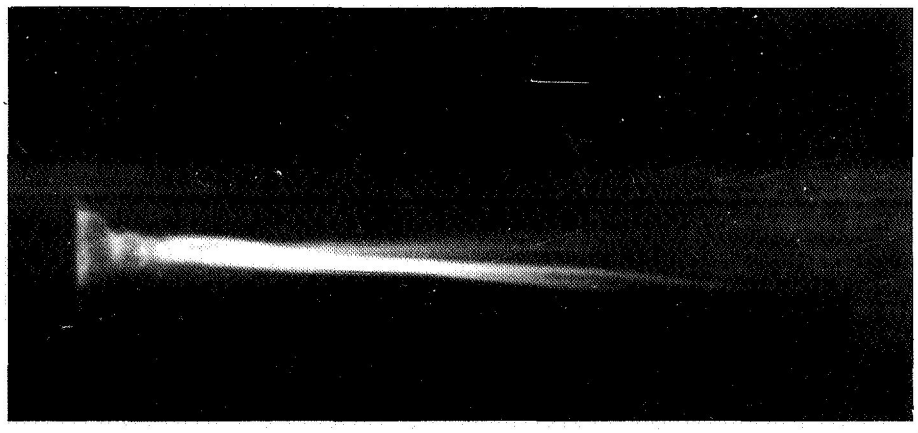

Figure 5.- Streak photograph of drift plotted in figure 4. L-68-10,075

bias field, the plasma rapidly escapes from the coil ends and the particle density at the axial center can be expected to decay markedly while the plasma column drifts.

The effect of such end losses can be included in the theory. Equations of state for an adiabatically compressed plasma with end losses have been derived in reference 5, and the following equation obtained from that reference describes a $\beta = 1$ plasma whose ions stream out the ends with mean thermal velocity:

$$T = T_\tau \left(\frac{N_\tau}{N}\right)^{3/10} \left(\frac{B}{B_\tau}\right)^{4/5} \tag{8}$$

In this equation, $B = B_{max} \sin \omega t$ and $B_\tau = B_{max} \sin \omega\tau$. The particle loss rate, which is just the efflux rate through a hole of area A (ref. 6), is represented by

$$\frac{dN}{dt} = 2 \frac{n\bar{v}_{th}}{4} A \tag{9}$$

where

$$\bar{v}_{th} = \sqrt{\frac{8\kappa T}{\pi m_i}} \tag{10}$$

and where the factor 2 is included because losses occur at both ends of the tube. Equations (8), (9), and (10) constitute a set which can be solved numerically for n. The result can be used in equation (7) to yield the loss-corrected drift. This process has not been carried out, however, since the necessary input parameters (temperature, volume, and especially hole area) are not known to an accuracy necessary to justify this degree of elaboration in the theory.

It should be noted that the drift of a theta-pinch plasma due to field gradients is not truly an instability of some equilibrium state but rather a nonequilibrium situation, the correction of which depends on the reduction of the field gradients to the point where the drift times are long compared with the half-cycle period of the compression field.

Rotational Instability

Several mechanisms leading to rotation of a magnetically confined plasma have been postulated. The instability by which this rotation is observed in a theta pinch takes the form of a fission of the plasma column into two strands which separate, go to the walls, and thus destroy the confinement. This effect is depicted in figure 6 by a line drawing taken from reference 7. The rotational instability has been observed photographically

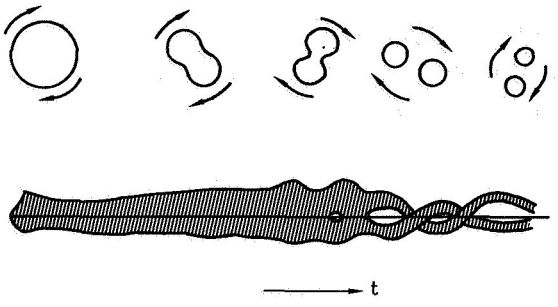

Figure 6.- Line drawing of streak showing m = 2 rotational instability.

both with side-on and end-on streak photography (refs. 8 to 11) and with end-on framing photography (refs. 8 and 11).

The effect is usually interpreted as an m = 2 Rayleigh-Taylor instability caused by the centripetal acceleration of the plasma column in the presence of the confining magnetic field. The single-fluid hydromagnetic description of this instability (ref. 12) leads to the dispersion relation

$$\omega_g^2 = -kg \tag{11}$$

where ω_g is the reciprocal of the growth time of the instability, k is the wave number, and g is the acceleration of the plasma. This relation predicts unstable solutions for all wave numbers. With the inclusion of finite ion cyclotron frequency and radius (see refs. 13 to 15) in the theory, the following equation for the stability criterion (given in the notation of the present paper) was obtained in reference 16:

$$\frac{k^2}{\Omega^2}\left(g + \frac{\overline{v}^2}{2\delta}\right)^2 \geqq \frac{4g}{\delta} \tag{12}$$

The thickness of the plasma boundary layer δ is defined as $\frac{n}{dn/dr}$. Equation (12) is valid only for $\beta = 0$, where $\beta = \frac{n\kappa T}{B^2/2\mu_o}$. However it can be shown by using the equations of reference 16 that the correction for finite β is negligible. The inequality may be solved for plasma acceleration to yield

$$\left.\begin{aligned} g &\geqq \frac{1}{2\delta}\left(4U^2 - \overline{v}^2 + 2\sqrt{2}U\sqrt{2U^2 - \overline{v}^2}\right) \\ g &\leqq \frac{1}{2\delta}\left(4U^2 - \overline{v}^2 - 2\sqrt{2}U\sqrt{2U^2 - \overline{v}^2}\right) \end{aligned}\right\} \tag{13}$$

where $U = \Omega/k$. For the rotational instability, $k \approx m/r_2$ where m is observed to be 2. By taking $B \approx 5$ teslas and considering a hydrogen plasma with $\overline{v} = 500$ km/sec and $\delta = 1$ centimeter, the range of unstable angular velocities is found to be

$$5 \times 10^6 \leqq \omega \leqq 3.9 \times 10^8 \tag{14}$$

which is in agreement with the observed unstable angular velocities (refs. 8, 9, 11, 17, 18, and 19).

The mechanism by which the plasma acquires angular momentum is not altogether clear. A large number of feasible mechanisms have been proposed to explain the phenomenon. These theories are discussed comparatively in reference 20. They can be classified according to how the reaction torque is taken up. Purely electromagnetic angular momentum as the reaction absorber (ref. 21) can be shown to be too small by four to eight orders of magnitude in a large theta pinch although it may explain rotation in a low-density mirror machine. Roberts and Taylor (see refs. 8 and 22) have suggested that the reaction is taken up by circulating currents at the wall and that the plasma is driven essentially by the electric field in the sheath. In reference 20 Haines has modified an earlier suggestion by Jensen and Voorhies (ref. 23) to show that viscous momentum transfer to the walls by ion-wall collisions may account for the rotation. Bostick and Wells (ref. 24) have suggested that plasma is expelled as vortex rings from either end while the remaining plasma, the toroidal velocity of which is opposite to that in the rings, coalesces in the center. Velikhov (ref. 25) has suggested a radial division of the plasma into oppositely rotating layers. The best supported theory is that of Haines in reference 26, where a model in which the reaction is absorbed by external conductors via the magnetic stresses is proposed. This model depends on the presence of a radial component of magnetic field with a nonvanishing azimuthal gradient. The ideas can be summed up in a simplified analysis written by the present author. An axial Hall current density j_z is generated by the interaction of the azimuthal current density j_θ with the radial component of the magnetic field. The Hall current then interacts with the radial magnetic field to produce an azimuthal force on the plasma column proportional to B_r^2. A simple statement of the generalized Ohm's law and Newton's second law yields

$$\frac{j_z}{\sigma} = \frac{j_\theta B_r}{ne} - v_\theta B_r \tag{15}$$

and

$$\rho \frac{dv_\theta}{dt} = j_z B_r \tag{16}$$

The first term on the right-hand side of equation (15) describes the axial Hall electric field. Equations (15) and (16) are combined to yield

$$\frac{dv_\theta}{dt} + \frac{\sigma B_r^2}{\rho} v_\theta = \frac{\sigma j_\theta B_r^2}{ne\rho} \tag{17}$$

which, with $v_\theta = 0$ for $t = 0$, gives for the rotational velocity

$$v_\theta = \frac{j_\theta}{ne}\left[1 - \exp\left(\frac{-\sigma B_r^2 t}{\rho}\right)\right] \tag{18}$$

Thus the limiting rotational velocity is appropriate to the velocity associated with diamagnetic current when j_z vanishes. If j_θ is reduced to less than nev_θ, the Hall current flows in the opposite direction and decelerates the rotation. Thonemann and Kolb (see refs. 3 and 20) have analyzed, with a computer, the full two-fluid equations including field distortion by the Hall currents and have found a time constant for the acceleration process given by

$$\tau = \frac{\rho}{\sigma B_r^2}\left[1 + \left(\frac{\sigma B}{ne}\right)^2\right] \tag{19}$$

A summary of the main features of these rotation mechanisms is taken from reference 20 and shown in table I, with the notation changed to that of the present paper. Strong experimental evidence has been found to support the Haines model of rotation that involves the external conductors. It has been shown in reference 27 that an externally applied transverse magnetic field of only 0.015 tesla is sufficient to induce rotational instability. Thus, the rotational instability and the drift of the plasma column have both been shown to depend critically on the nonuniformity of the magnetic compression field.

Other Instabilities

The instabilities discussed in the two preceding sections constitute the most dangerous of the instabilities which beset the theta pinch in the sense that they limit the confinement time to a quarter or less of the coil-current oscillation period. The theta pinch also exhibits a rich variety of less drastic instability phenomena which are now briefly discussed for the sake of completeness.

A "wobble" instability was found in the Culham Laboratory theta-pinch experiment (ref. 28). This instability manifests itself as a spiral precession of the center of the plasma column. It has been suggested that wobble instability is due to slow rotation of the plasma column (below the threshold for the $m = 2$ instability) and to magnetic line-tying between the column and currents at the vacuum-chamber wall. Line-tying gives

TABLE I.- PRINCIPAL FEATURES OF ROTATION MECHANISMS

Location of mechanical reaction	Hall currents or stress tensor	Carrier of reaction	Plasma isolated?	Azimuthal symmetry?	Predicted angular frequency	Approximate acceleration time	Necessary conditions and name of originator
Wall of containing vessel	Hall currents (radial)	Electrons	No	Yes	$\frac{cB}{4N}\frac{1-\sqrt{(1-\beta)}}{Ze}$ to $\frac{ZeB}{2m_ic}$	$\frac{\rho c^2}{\sigma B^2}\left[1+\left(\frac{\sigma B}{nec}\right)^2\right]$	Electrical contact with conducting walls to obtain circulating currents (Roberts and Taylor)
Wall of containing vessel	Stress tensor	Ions	No	Yes	$\frac{1}{R^2}\frac{kTc}{ZeB}$	$\frac{m_ic}{ZeB}$	Physical contact with wall for a time greater than a fraction of an ion Larmor period (Haines)
External conductors	Hall currents (axial)	Magnetic stress tensor	Yes	No	$\frac{j_\theta}{rne}$	$\frac{\rho c^2}{\sigma B_r^2}\left[1+\left(\frac{\sigma B}{nec}\right)^2\right]$	Presence of azimuthally varying radial magnetic field of sufficient amplitude (Haines)
Plasma at each end of discharge axis	Hall currents (radial)	Electrons	Yes	Yes	0 to $\frac{ZeB}{2m_ic}$	$\frac{\rho c^2}{\sigma B^2}\left[1+\left(\frac{\sigma B}{nec}\right)^2\right]$	Magnetic field lines diverging at each end of coil and axial loss of oppositely rotating plasma (Bostick)
Plasma nearer the discharge axis	Stress tensor	Ions	Yes	Yes	$\approx\frac{1}{R^2}\frac{kTc}{ZeB}$	$\frac{m_ic}{ZeB}$	A large change in ion diamagnetic current; inside plasma rotates in opposite direction (Velikhov)

an effective friction with the wall. As the plasma column drifts off the magnetic axis, some of the column spin becomes transformed into orbital angular momentum of the center of mass. The column is not observed to strike the wall within the confinement time.

In reference 29 it has been predicted that a theta-pinch plasma with reversed trapped field would be subject to a resistive instability resulting in a "tearing"-mode breakup (breakup along current-flow lines) of the column into short rings. This process has been observed in reference 30 and is illustrated in figure 7. In experiments in which short coils are used, the current layer often collapses into a single ring (ref. 8), presumably because the tearing mode which grows fastest for long wavelengths does not have room or time to establish itself. For longer coils, as many as seven rings appear (ref. 30) and subsequently coalesce as axial contraction of the plasma column occurs. It has been suggested that vortex rings of the Alfvén wave type (ref. 31) similar to those observed in references 32 to 36 may be present in the Langley theta pinch. Transverse striations are seen in the streak photographs of figures 3 and 5 (taken side-on). The initial striations are dependent on the magnetic field strength and the linear mass density of the plasma (ref. 37) and are strongly damped as a result of plasma heating by magnetic pumping (ref. 38). A series of striations of different period follow the initial striations and show much less damping. A microdensitometer trace of a streak photograph illustrating these effects is shown in figure 8, where the film density is recorded along the center line of the plasma image. The plasma from which these data were taken had no trapped field; hence one would not have expected the tearing-mode instability to develop. It is unlikely that the observed series of striations of different period are associated with radial oscillations as are the initial oscillations, since no modulation of the plasma radius is evident. Rather, they are tentatively interpreted as magnetovortices generated by a resistive "rippling" mode (ref. 29) that propagate along the plasma column with Alfvén speed. This interpretation has not been verified since poloidal flows necessary for confirmation would have to be detected by probe measurements and such measurements are impractical in such a high-energy plasma (refs. 39 and 40). Velocity measurements, however, may be possible.

In short coils, axial magnetic-line tension tends to concentrate the plasma into a single short ring which subsequently seeks to flip over so as to aline its trapped field with the magnetic compression field (see ref. 41). This instability has been analyzed in reference 42 where plasmas with sufficiently high length-radius ratios are shown to be stable with respect to flipping.

Azimuthal and axial striations have been observed in the photographs presented in references 18, 43, and 44. Also, Rayleigh-Taylor instabilities (flutes) are evident in end-on framing photographs in these references. It has been suggested that these long

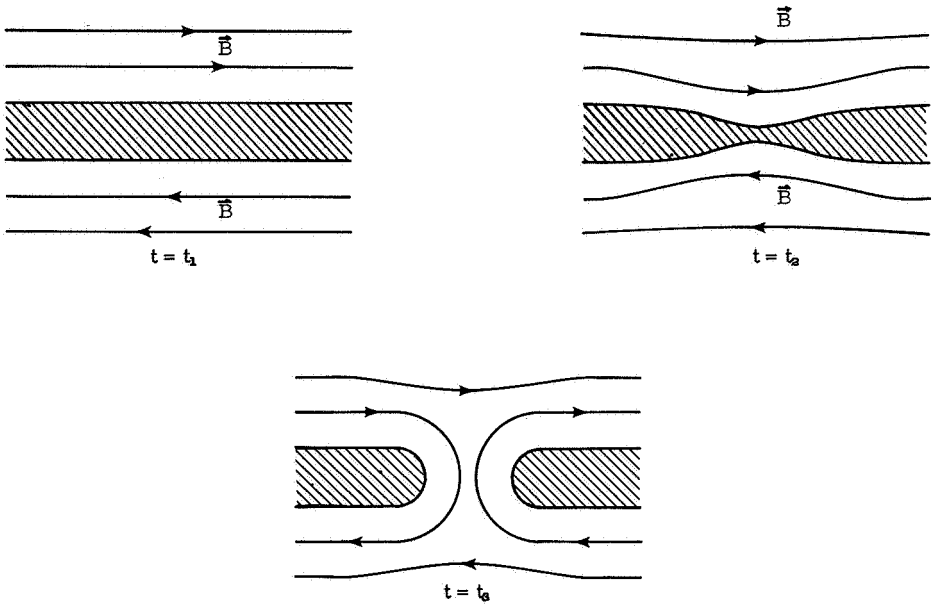

Figure 7.- Development of the tearing-mode instability; $t_1 < t_2 < t_3$.

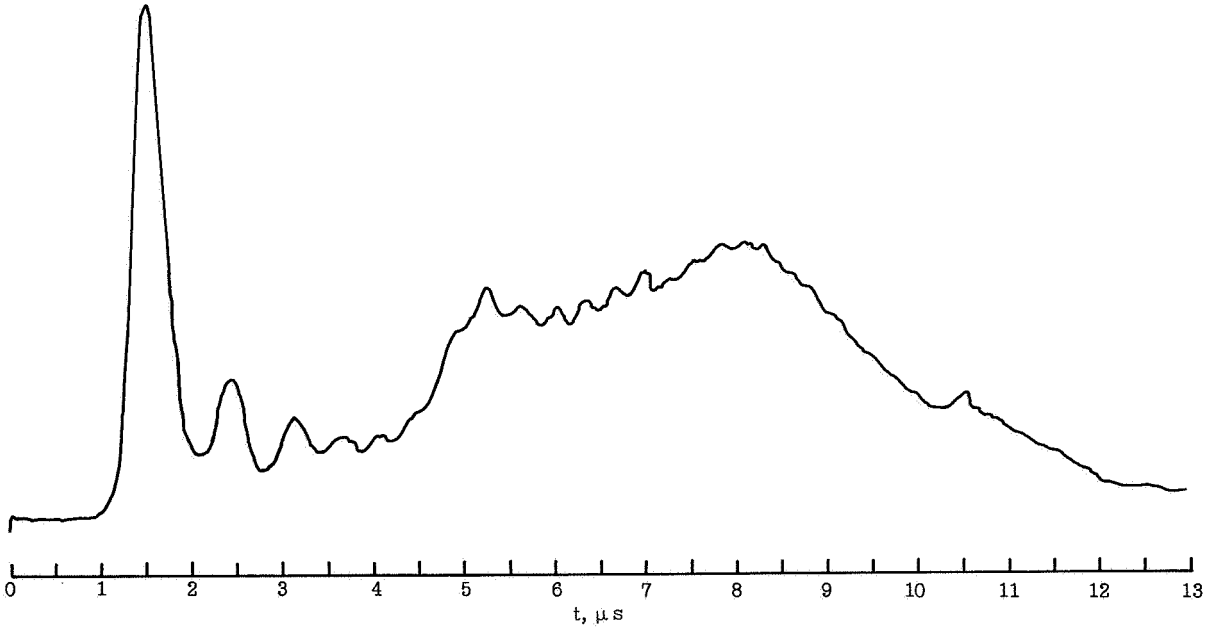

Figure 8.- Microdensitometer tracing of plasma streak photograph.

serpentine flutes may be due to helical kinks in the axially alined striations. An analogy to a rope twisted under tension might be made; kinks appear as the tension is relaxed.

SOURCES OF FIELD NONUNIFORMITY IN A THETA-PINCH COIL

As the foregoing discussion points out, the most harmful of the plasma instabilities which occur in a theta pinch – that is, the drift and rotation – are caused and/or aggravated by nonuniformity in the magnetic compression field. There can also be effects due to lower electrical conductivity of the plasma caused by the presence of impurities of high nuclear charge. In reference 27 it has been shown that the presence of as little as 0.1 percent of contaminant of high nuclear charge can cause explosive rotational instability. If the contamination is appreciable, the electron temperature (and hence the electrical conductivity which varies as $T^{3/2}$) will be seriously degraded by radiation. For high densities such that the ions are effectively coupled to cold electrons, the finite-gyroradius stabilization of a rotating flute would be less effective (see ref. 15). In addition, the magnitudes of the torques which drive the rotation depend on the electrical conductivity (ref. 3). In the drift the effect of contamination is not so drastic. The magnetic moment can be altered somewhat by changes in the skin depth of the plasma and there can also exist secondary effects, which are discussed subsequently. The problem of minimizing contaminants of high nuclear charge is essentially one of vacuum technology and proper gas injection and is not discussed herein. Rather the present discussion is concerned with the causes of field nonuniformity in a theta-pinch coil.

The requirement for connecting a large number of coaxial cables (up to 1000) to a single-turn coil about 1 meter in length dictates the geometry to a large extent. In the Langley magnetic compression experiment as well as in the NRL experiment, a pair of large (4.8 by 1.2 meters) current-collector plates are used with the cables connected to one of the long sides and the coil symmetrically attached to the other. This system is shown schematically in figure 9. Figure 10 is a photograph of the Langley magnetic compression experiment. The lead bricks on the collector plates are necessary to limit the amplitude of the bouncing of the plates when the current pulse passes through them. The plates are further restrained by 128 steel bolts. The coil is shown in the center of the photograph and in more detail in figure 11. Also shown in figure 10 are the rotating-mirror streak camera and a spectrograph. By considering this general configuration to be typical of large theta pinches, several major sources of magnetic-field inhomogeneity can be delineated.

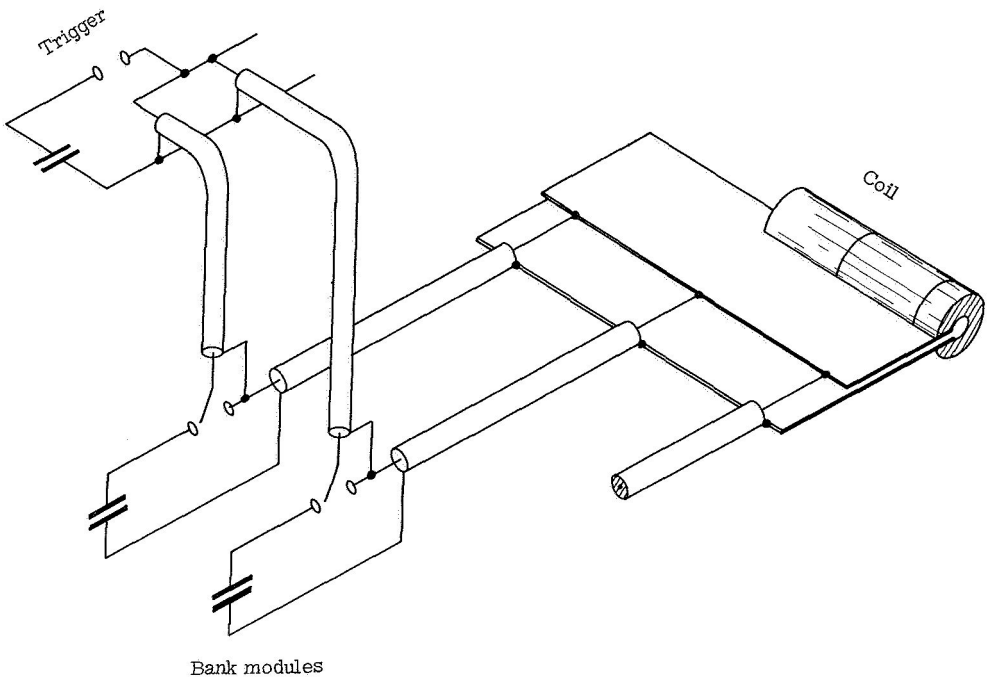

Figure 9.- Schematic diagram of the capacitor bank and collector-plate system.

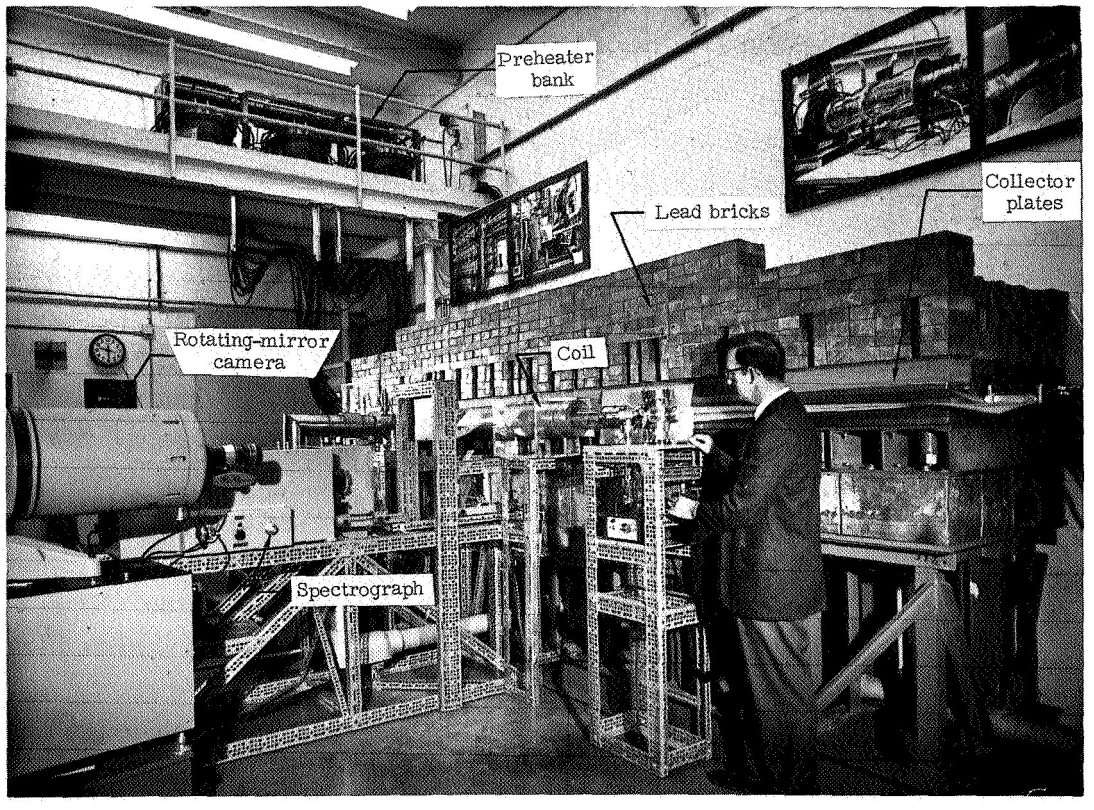

Figure 10.- The Langley magnetic compression experiment. L-64-11,106.1

Collector Geometry

Figure 12 shows a resistive analog plot of the field lines to be expected in the collector plates of the Langley magnetic compression experiment. The two plates have been unfolded about the coil in order to create a planar surface. The equipotential pattern shown corresponds to magnetic field lines in the limit of dc operation, since the magnetic field can be described in current-free space by a scalar potential which obeys the Laplace equation. The reproduction of the ac conditions occurring in the experiment (skin depth much less than conductor thickness) is technically unfeasible in the analog plot and hence the region near to and including the coil is not altogether accurately represented.

The top plate is slotted perpendicular to the long sides, as shown in figure 12, in order to provide a high inductance path to inhibit destructively high currents in case of a short circuit between the plates. The holes are provided to bolt the plates together.

The field pattern on the left side of the center line is obtained with current supplied only to the center third of the plates. The pattern on the right side is obtained with current supplied to the entire length of the plates. The field lines near the coil-collector interface show considerable curvature under both conditions – that is, the current has a nonnegligible component parallel to the coil axis. It is this "funneling" effect of the current and the consequent gradient of the field in the coil that probably contribute most to drift instability in large theta pinches.

As pointed out in reference 2, the curvature may be aggravated by too large a coil feed slot. Since curved field lines in the coil may bend into it, this slot should be minimized in order to minimize the curvature.

Another source of field gradient due to the collector geometry may be the large volume external to the coil from which the field is excluded. The collector plates and their supporting structure together with the lead bricks, all on one side of the coil (see fig. 10), exclude the high-frequency field from this volume and thus one might expect some degree of azimuthal asymmetry of the field also in the coil interior. It is suggested in reference 45 that the effect might be fairly large in the end regions. For long coils, as is shown subsequently, the ratio of magnetic field outside the coil to magnetic field inside the coil is on the order of only a few percent; hence the field stresses, which vary as B^2, are almost four orders of magnitude less on the outside than on the inside. Thus deviations from homogeneity of the inside field far from the end (e.g., in the median plane) due to external azimuthal asymmetry should be less than 0.1 percent. In reference 46 the introduction of large metal plates at the ends of the coil to partially balance the azimuthal symmetry was noticed to cause some difference in drift rate. A similar configuration had been tried previously and no such effect observed, so the question of the influence of end plates on drift remains an open one.

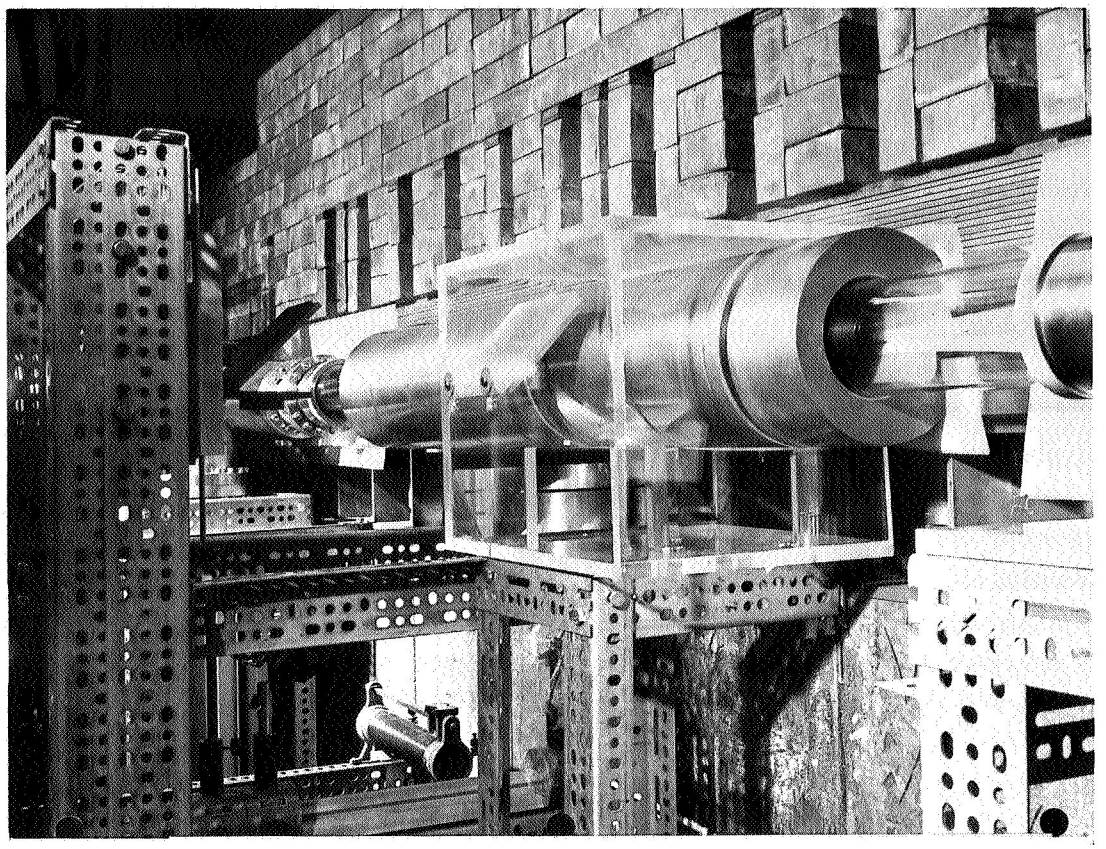

Figure 11.- Closeup of coil in Langley magnetic compression experiment. L-64-11,103

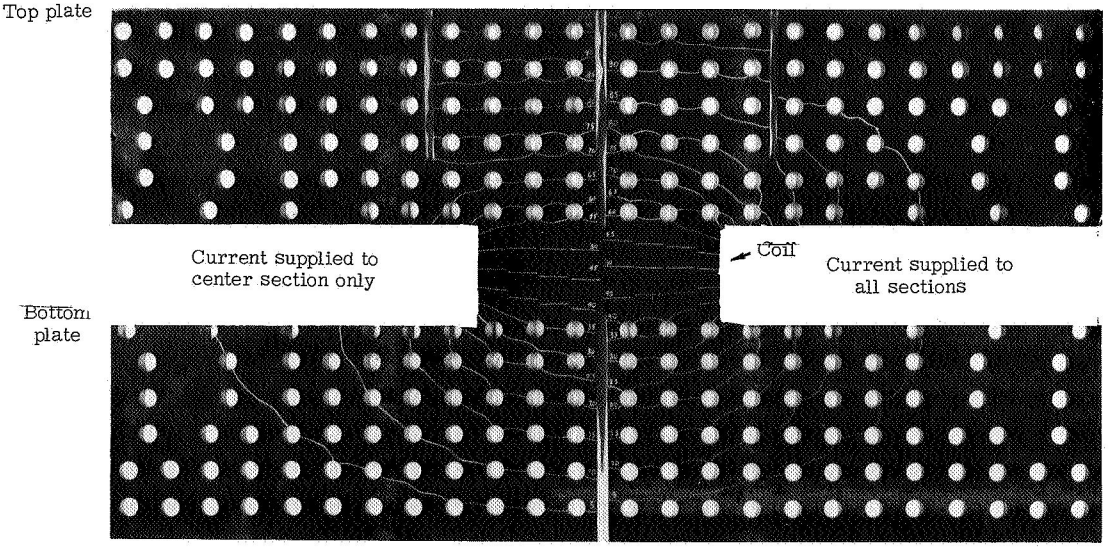

L-68-10,076

Figure 12.- Resistive analog plot of magnetic field lines in the collector plates of the Langley magnetic compression experiment.

Plasma Shape

When the plasma contracts axially such as to concentrate itself near the median plane of the coil, that portion of the coil has lower inductance and the driving current converges there. The effect is similar to the current funneling just discussed. The field lines have a curvature that is convex toward the coil slot, and the plasma may be expected to drift in that direction.

The axial contraction is usually observed to be a strong effect only in plasmas employing a reversed bias field. As shown previously herein, resistive instabilities and/or vortex coalescence may serve to cause axial contraction. It can be shown that a tubular plasma corresponds to an equilibrium state and that tension of the axial field lines should not cause contraction. Thus an instability of some sort must provide a mechanism to trigger the contraction. The problem has been investigated in the Langley theta pinch by examining the plasma with the use of light pipes (fiber bundles) spaced every 15 centimeters along the coil axis. The ends of the light pipes away from the axis form a continuous slit which is focused on the photocathode of an image-converter streak camera. The monitoring system, which is similar to one used at Langley Research Center to study spark-gap jitter (ref. 47), is shown in figure 13. Figure 14 is a typical axial-light-intensity streak record. The sinusoidal shape is due to perturbation of the electron optics in the image-converter tube caused by the magnetic field of the discharge and actually allows direct comparison of the axially resolved light intensity with the discharge current. A trace shows that axial contraction begins roughly 5 μs after the start of the

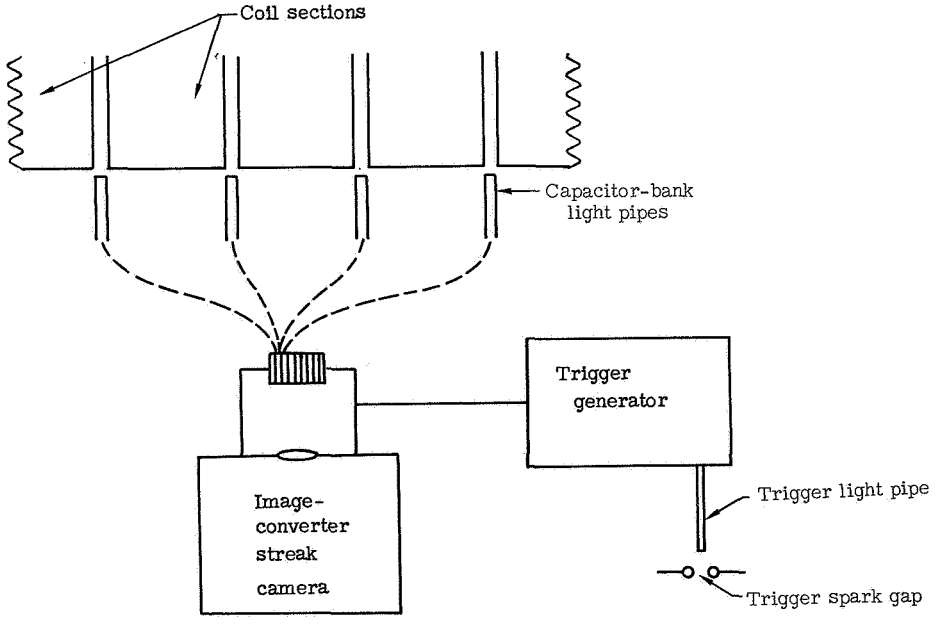

Figure 13.- Axial-light-intensity monitoring system.

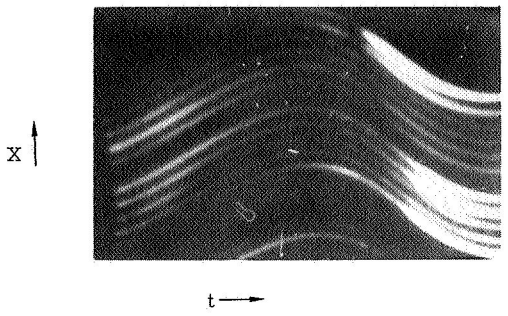

L-68-10,077
Figure 14.- Axial-light-intensity streak record.

discharge. The ends appear to move in with a speed of approximately 5 cm/μs until the column has contracted axially to a length of approximately 40 centimeters. Illumination in the end regions due to end losses builds up until, near the end of the first half-cycle, the plasma streams out at the coil ends, follows the flaring magnetic field, and strikes the walls. Impurity line radiation greatly intensifies at that time. With large end losses, there is difficulty in determining whether it is axial contraction or an axially propagating rarefaction wave that is observed. The effect on the magnetic field is, however, the same. The second half-cycle is largely overexposed as a result of the intense line radiation. These phenomena correspond rather closely with those observed in reference 27 for the NRL experiment. The plasma contraction is apparently limited to a minimum length of about a third or a quarter of the initial column length. The observed plasma radius does not seem to change in this time; thus for the high compression ratios employed (approximately 100:1), the change in inductance should be moderate. In a short coil where the axial contraction is a stronger effect, the perturbation on the field may be significant.

End Effects

Because of the finite length of the coil, the field lines diverge and thus produce an azimuthally symmetric radial gradient which increases as one approaches the end of the coil from the center. This field pattern is not the same as for the dc solenoid where flux can permeate the coil wall. For the ac conditions (skin depth much less than radial coil thickness), the field pattern is approximately that depicted in figure 15, where the

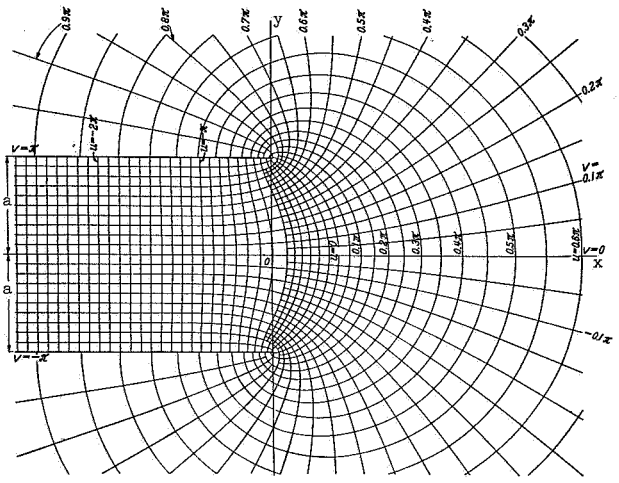

Figure 15.- Maxwell curves obtained from equation $z = \frac{a}{\pi}\left(w + 1 + e^{w}\right)$.

constant-v lines represent the magnetic field lines. The coil is considered to be semi-infinite. A Schwarz-Christoffel transformation yields the mapping from this two-dimensional geometry to the Cartesian coordinate system. The equation for the Maxwell curves is found to be (ref. 48)

$$z = \frac{a}{\pi}\left(w + 1 + e^{w}\right) \tag{20}$$

where

$$\left.\begin{aligned} z &= x + iy \\ w &= u + iv \end{aligned}\right\} \tag{21}$$

with $i = \sqrt{-1}$. Equation (20) can thus be written as

$$x = \frac{a}{\pi}\left(1 + u + e^{u}\cos v\right) \tag{22}$$

or

$$y = \frac{a}{\pi}\left(v + e^{u}\sin v\right) \tag{23}$$

These equations may be inverted by numerical iteration in order to find $\partial v/\partial y = g(x,y)$ from which $B(r,x)$ may be obtained. The results are shown in figure 16 where, with x being the distance into the coil from the end, the ratio of $B(r = 0,x = 0)$ to $B(r = 0,x = \infty)$ – that is, B/B_{∞} – is plotted as a function of r/a where a is the coil radius. Further calculations show that B/B_{∞} approaches unity to within 0.1 percent at a distance of two radii from the end. This result supports the use of a semi-infinite coil length in the calculation instead of a finite coil length. Thus stabilization against drift due to the "minimum B" magnetic well is confined to the very ends of the coil and cannot be expected to be effective in large experiments where the coil aspect ratio (ratio of coil length to radius) is greater than 20. The fact that the calculated mirror ratio $\frac{B(r = 0,x = 0)}{B_{\infty}}$ agrees within a few percent with the measured value gives some degree of confidence in the two-dimensional model.

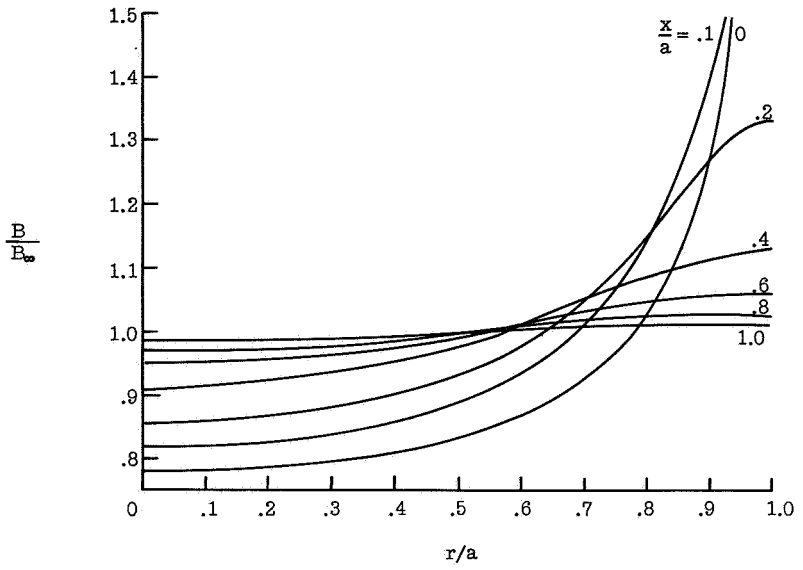

Figure 16.- Magnetic contours at the end of a semi-infinite coil.

As shown in reference 49, the plasma drift may be calculated from the point of view of orbit theory as well as by use of a magnetohydrodynamic model. The orbit-theory analysis in reference 49, although correct, involves currents and thus is somewhat a hybrid. The following analysis by the present author is therefore preferred. The equation for the velocity of particle drifts that cause charge separation (obtained with the use of ref. 16) is

$$w = \frac{m_i}{qB^2}\left[\left(v_{||}^2 + \frac{v_\perp^2}{2}\right)\nabla B - \dot{E}\right] \tag{24}$$

where the time rate of change of the electric-field strength is given by

$$\dot{E} = \frac{nqw}{\epsilon_o} \tag{25}$$

Combining these equations to eliminate w, one finds

$$\dot{E} = \frac{\frac{nm_i}{\epsilon_o B^2}}{1 + \frac{nm_i}{\epsilon_o B^2}}\left(v_{||}^2 + \frac{v_\perp^2}{2}\right)\nabla B \tag{26}$$

where $1 + \frac{nm_i}{\epsilon_o B^2}$ is the plasma dielectric constant, which is large compared with unity.

Thus equation (26) reduces to

$$\dot{E} \approx \left(v_{||}^2 + \frac{v_\perp^2}{2} \right) \nabla B \tag{27}$$

The zero-order electric drift which acts on the plasma as a whole is given in reference 16 by

$$w^E = \frac{E \times B}{B^2} \tag{28}$$

Thus the following equation can be written:

$$\ddot{r} = \dot{w}^E = \left(v_{||}^2 + \frac{v_\perp^2}{2} \right) \frac{\nabla B}{B} \tag{29}$$

The term involving dB/dt has been neglected in equation (29) inasmuch as the reciprocal of the time for polarization of the plasma v_{th}/r_2, where v_{th} is the thermal velocity of the ions and r_2 is the radius of the plasma column, is typically two orders of magnitude larger than the angular frequency of the magnetic flux density ω. With

$$\frac{\nabla B}{B} = \frac{1}{R} \tag{30}$$

$$v_{||}^2 + \frac{v_\perp^2}{2} = \frac{2\kappa T}{m_i} \tag{31}$$

and, for the assumption of a $\beta = 1$ plasma,

$$2n\kappa T = \frac{B^2}{2\mu_o} \tag{32}$$

equation (29) can be written as

$$\ddot{r} = \frac{B^2}{2nm_i \mu_o R} = \frac{\pi B^2 r_2^2}{2M\mu_o R} \tag{33}$$

which is, within a factor 1.5, the same as equation (5) with $B_r = r_1 = 0$.

The point of this analysis is that there exists a polarization in the drifting plasma, at a right angle both to the direction of drift and to the magnetic field, whose sign is determined by the direction of the curvature. In reference 50 it has been found that in a theta pinch of moderate length, considerable curvature can be tolerated without drift. This result has been verified in reference 51. The explanation is that gradients reverse in the end regions, particularly for those coils which feature magnetic mirrors. Thus the polarity of the charge separation in the end regions is opposite to that near the coil center. The electron conduction along magnetic field lines allows the fields to be short-circuited. (See fig. 17.) This effect has been demonstrated very dramatically in reference 50 by isolating the end regions from the main body of the plasma with the use of glass plates. The plasma then drifts rapidly to the wall.

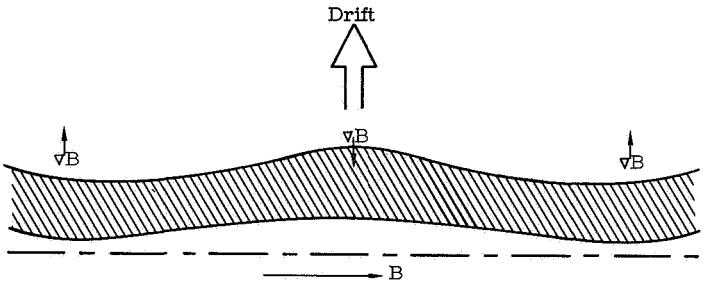

(a) Top view, with polarization normal to the page.

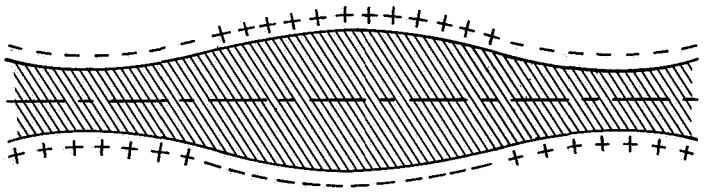

(b) Side view showing reversal of polarization due to inflection in curvature of field.

Figure 17.- Polarization effect on drift.

Coil-Collector Discontinuity

In the high-frequency limit (i.e., with the skin depth δ much less than the thickness of the conductors), the partition of the current between the inside and outside surfaces of the plates in a parallel-plate transmission line is a function of the gap spacing h and the width of the transmission line b. As pointed out in reference 2, a variation of the ratio h/b along the length of the transmission line causes current to spill around the ends in order to adjust the current ratio (ratio of current outside to current inside) to the value necessary for maintaining a constant skin depth. This effect is of interest herein

since the collector plates, coil slot, and coil form a transmission line with abrupt changes in h/b.

As the current flows from the coil slot ($h/b \approx 0.001$) into the coil ($h/b \approx 0.1$), the value of h increases from 1 millimeter (at the slot) to 10 centimeters (the coil inner diameter). Part of the current flowing on the inner surface must then spill around the ends of the coil.

The ratio of current outside to current inside may be computed from equations (22) and (23). The quantity $\partial v/\partial y$ at $y = a$ (for $v = \pi$) is required (see fig. 16). Setting $v = \pi \pm \theta$, where θ is small, and expanding to first order yields

$$x = \frac{a}{\pi}(1 + u - e^u) \tag{34}$$

and

$$y = \frac{a}{\pi}\left[\pi \pm \theta(e^u - 1)\right] \tag{35}$$

for which

$$\frac{\partial \theta}{\partial y} = \frac{\partial v}{\partial y}\bigg|_{v=\pi} = \pm\frac{\pi/a}{e^u - 1} \tag{36}$$

Equations (34) and (36) serve to determine the ratio of magnetic-field strength at any axial location in the coil. In order to find the ratio of total current outside to total current inside, one must integrate equation (36) with respect to x by means of equation (34). However since $x = 0$ corresponds to $u = 0$, equation (36) is singular at the origin. Physical arguments are advanced in the next section to determine the lower limit on this integral. As an indication of the magnitude of the current partition, the ratio of magnetic-field strengths can be compared at the median plane of the transmission line by setting $x = b/2$ in equation (34). The results, with values appropriate to the Langley experiment, are shown in figure 18. The effect on the field gradient in the coil due to this spilling of current around the ends is opposite to that induced by the collector geometry – that is, the gradient is directed toward the slot instead of away from it.

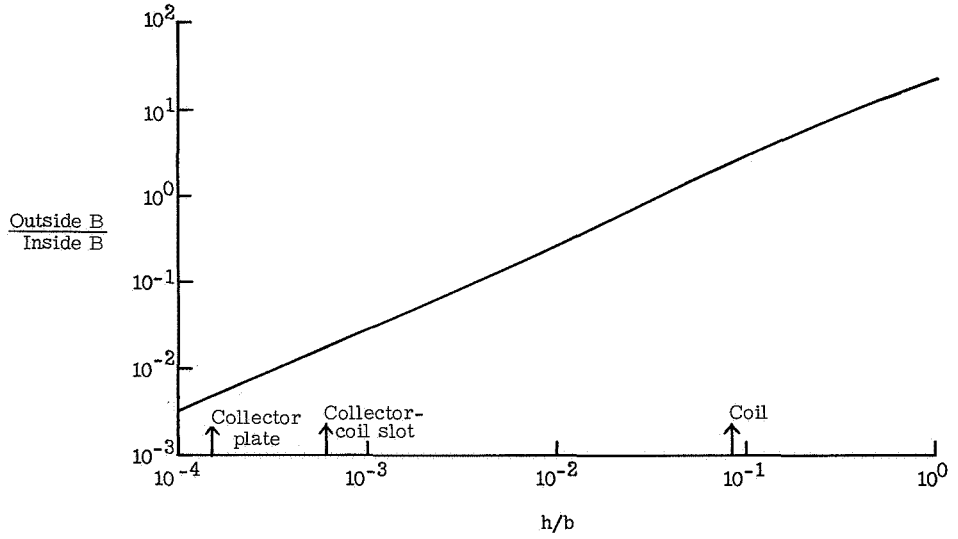

Figure 18.- Divergence of the current from the inside to the outside of a parallel-plate transmission line for $x = b/2$.

Axial Current Distribution

The axial distribution of current in a high-frequency coil is not uniform as in the dc case. Equations (34) and (36) may be used to calculate the axial distribution. The current-density variation near the end of the coil is given in figure 19. In practice, the limiting value of the current density is determined by the coil material through the requirement that the heat generated at the conductor surface by joule losses not melt the coil material. This requirement is equivalent to specifying a minimum radius of curvature of the edge at the end of the coil. As shown in reference 52, the limiting value of a sinusoidally varying, high-frequency magnetic field that can be tolerated at the surface of a conductor can be given by the relation (in notation of present paper)

$$\Delta T = \frac{B_{max}^2 \pi}{2\mu_o c_v} \qquad (37)$$

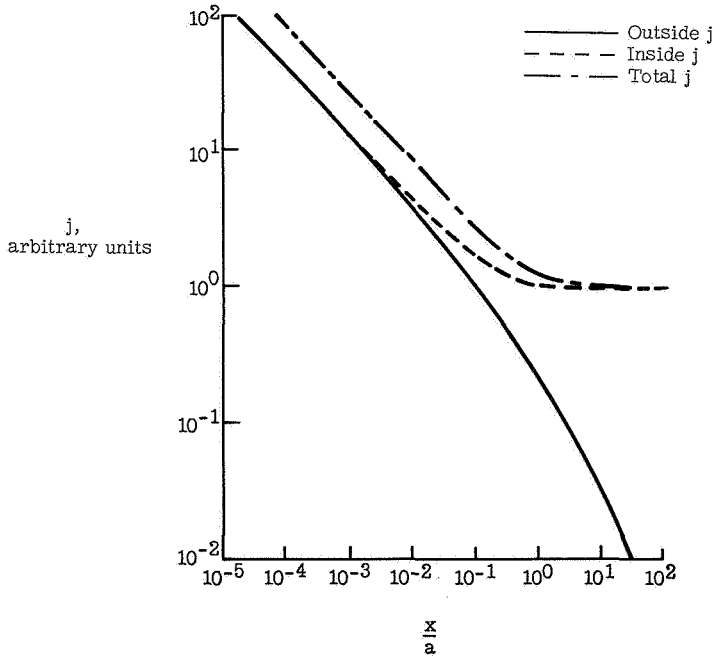

Figure 19.- Current-density variation near the end of the coil.

where ΔT is the temperature gain per half-cycle of the current oscillation, B_{max} is the peak magnetic flux density at the coil surface, and c_v is the specific heat per unit volume. For the beryllium-copper coil used in the Langley experiment the maximum tolerable field, with 1 half-cycle of operation assumed, is 54 teslas. In order for the Langley coil to be used with the full capability of the capacitor bank (12.6 megamperes), the edge of the coil end must be rounded to approximately 0.5 millimeter. If the edge is not rounded, the field itself will round the corner to conform to the 54-tesla field contour. This effect has been recorded photographically. During about the first hundred shots of the coil, sparking from the edges was observed. As the coil edges eroded, the sparking diminished until there was no point on the coil where the surface field exceeded the critical value.

Thus the partitioning of the total current between the inside and outside surfaces depends not only on h/b but also on the value of the total current. The determination of the current ratio involves numerical solution of an integral of the form

$$I_{total} = 2A\int_{X}^{b/2}\int_{0}^{t} \exp\left(-\frac{z}{\delta}\right)\frac{\partial v}{\partial y}(x)\,dx\,dz \tag{38}$$

where t is the thickness of the coil wall, δ is the skin depth $\sqrt{\frac{2}{\mu_o \omega \sigma}}$, X is the radius of curvature of the coil end $\left(\text{itself a function of } I_{total}\right)$, and A is the constant to be determined. The integration must be performed for $u > 0$ (the outside surface) and $u < 0$ (the inside surface).

As the current flows from the collector through the feed slot into the coil, an increasing percentage of the total current is channeled away from the median plane, inside as well as outside. This facet of the current redistribution phenomena reinforces the effect of current transfer described in the preceding section. The field gradient is directed toward the feed slot in opposition to the effect of current funneling.

METHODS OF PLASMA STABILIZATION

Evidence that major instabilities of theta-pinch plasma are caused by nonuniformity of the magnetic field as well as by the presence of impurities has been presented. The problem of reducing impurities involves advanced vacuum technology and the design of a high-purity-gas filling system such as the palladium or nickel leak which can be used to admit hydrogen or deuterium. This aspect of the problem is, however, not within the scope of the present work. The source of the field nonuniformity has been discussed. The major contribution to drift toward the feed slot (which is the dominant direction of

drift) seems to be the current funneling caused by the collector geometry. Axial contraction of the plasma column probably contributes also. The magnitude of the plasma-axial-contraction effect is difficult to ascertain since there are also end losses and the situation has not yet been described accurately by theory. Drift away from the feed slot, which is observed to be a smaller effect (ref. 2), is normally caused by current redistribution. Drift away from the feed slot has been observed in the Langley experiment in a plasma with reversed trapped field. The drift is reversed before the outer wall is reached and motion toward the feed slot ensues. (See fig. 20.) This effect seems to occur only when a reversed trapped field is used. The most likely explanation is that instabilities connected with the reversed-field configuration somehow enhance the motion of plasma toward the ends where it apparently is strongly concentrated, with an effect just opposite to that observed when the plasma contracts axially. The turn-around is caused by the expulsion of the plasma at the ends and/or by forces that arise as the plasma approaches the conducting wall of the coil (see refs. 53 and 54).

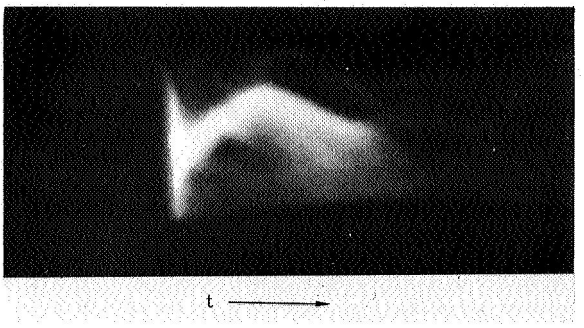

L-68-10,078
Figure 20.- Streak photograph showing retrograde drift in plasma with reversed trapped field.

It has been found in the Langley experiment that the rotational instability does not prove troublesome during the first half-cycle. After the plasma strikes the wall as a result of drift or the oscillation of the field, rotation is noted immediately on the following half-cycles and the plasma is violently unstable. Only the first half-cycle is used for observation; thus the drift constitutes the only disturbance which seriously limits the experiment.

The practical approaches to the solution of the instability problem in theta pinches are typified by the methods employed at NRL and at Culham Laboratory. Initially, NRL (see refs. 4 and 55) and Los Alamos Scientific Laboratory (see ref. 56) both used an Ioffe (ref. 57) hexapole magnetic field in an attempt to center the plasma column. The radial magnetic field associated with the Ioffe bars strongly excited the rotational instability, and thus this method had to be abandoned. Next, NRL built an extension to its collector-plate system, with a width equal to the coil length and with a length of 1 meter. This extension was found to reduce the measured value of $\Delta B_Z/B_Z$ of 0.1 percent by approximately a factor of 10 (see ref. 27). There are strong disadvantages to such an extension, however.

The coil inductance in a large theta pinch is typically about 7 nanohenries. In order to get a reasonable fraction of the bank voltage applied to the coil, the parasitic inductance

must be kept down to about 2 nanohenries. The parasitic inductance added by the collector-plate extension is

$$L = \frac{\mu_0 l d}{w} \tag{39}$$

where l is the extension length, w is the extension width, and d is the extension gap spacing. For a square extension (l = w) and a 1-millimeter gap spacing, the inductance would be about 1 nanohenry. Thus the voltage at the coil (upon which the ion heating by shocks depends) would be seriously degraded. In addition, the channeling of large currents would produce extremely high mechanical forces. The force between the plates would be

$$F = \frac{\mu_0 I^2 l}{2w} \tag{40}$$

With a mass loading M on the plates (usually consisting of lead bricks), the amplitude of the bouncing – that is, the maximum gap spacing – can be computed to be

$$d_{max} = \frac{\mu_0 I^2 l \tau^2}{4wM}\left(\frac{\mu_0 I^2 l}{2wMg} + 1\right) \tag{41}$$

where g is the acceleration of gravity and τ is the duration of the current pulse (assumed to be a square pulse). For a 1-meter-square extension with 10 megamperes of current for 20 μs and a mass loading of 10 000 kilograms, the amplitude of bouncing is approximately 1 millimeter. This bouncing causes severe hammering of the insulation.

It should be noted that although the current-funneling effect is adequately compensated, a simple extension does not cancel field nonuniformity caused by the coil-collector spacing discontinuity. In this respect the approach at Culham Laboratory (see ref. 2) is somewhat more sophisticated. A short extension which houses an inductive lens is used. (See fig. 21.) The inductive lens is an interchangeable section of the collector which has an increased inductance. The inductance varies across the width of the tab extension in such a way as to compensate for the convergence of the current paths in the coil. The objections which have been raised for the simple extension apply to this method as well, but the advantage of this technique lies in its flexability.

The solution being pursued in the present paper involves the use of flux concentrators (ref. 58). A flux concentrator is a metal cylinder with an axial slot which may be used to adjust the inductance of a pulsed coil and to concentrate the magnetic field into a smaller volume. (See fig. 22.) The axial current components in the coil are antiparallel above and below the coil feed slot. The presence of the slot prevents these components from canceling each other out. The flux concentrator which is introduced into the coil

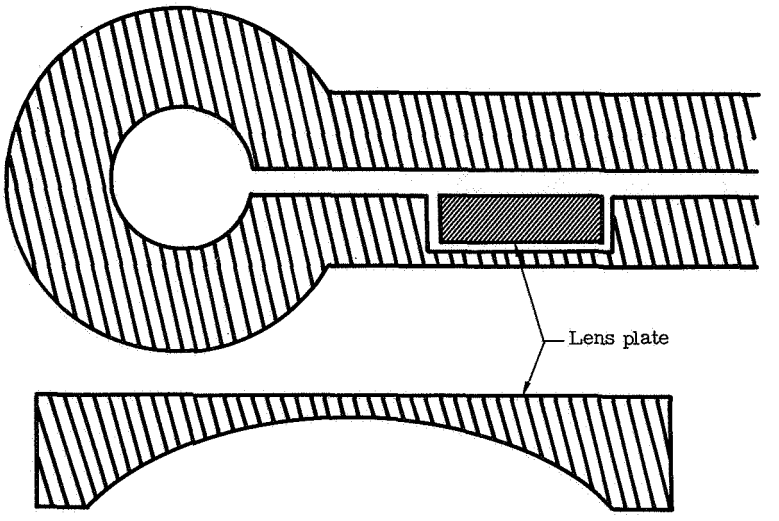

Figure 21.- Inductive lens for drift correction.

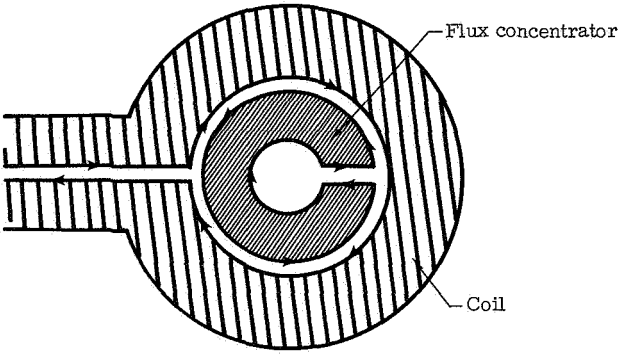

Figure 22.- Diagram showing cross section of flux concentrator in coil.

has its slot located on the opposite side from the coil feed slot. Thus the axial current components produced on the outer skin of the flux concentrator can cancel each other in closed loops. Only the azimuthal current components can reach the interior of the flux concentrator and be seen by the plasma. (See fig. 23.) This method not only reduces field nonuniformity due to current funneling but also, provided the radial thickness of the concentrator is not too large, guards against the current-transfer effect. (The radial thickness of the flux concentrator should be large compared with the skin depth, however.) In fact, the flux concentrator should cancel any axial current which is symmetric about the median plane. Currents which cross the median plane may be caused by bank jitter; however, the sort of switch commonly employed has jitter of less than 50 nanoseconds, so these effects are presumably small.

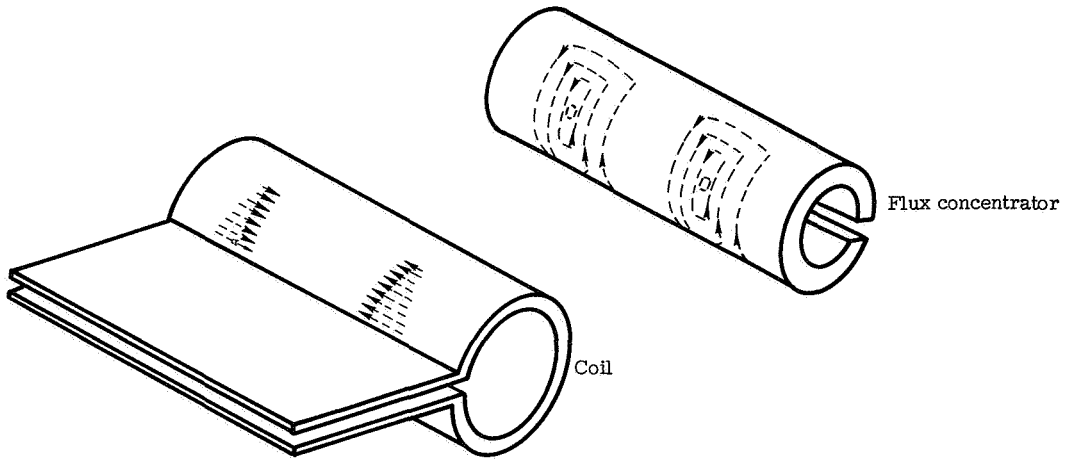

Figure 23.- Flux concentrator for shielding axial coil currents.

THE FIELD-SHAPING EXPERIMENT

A 1/2-scale replica of the Langley theta pinch has been built in order to measure the vacuum-magnetic-field distribution in the theta-pinch coil. Such an auxiliary facility is useful for evaluating the effect on field uniformity of various coil-collector geometries. In particular, the relative merits of collector-plate extension and flux concentrator can be compared.

Description of Experimental Apparatus

In order that the scaling include not only the geometry but also the skin depth, variable inductors are added in series with the collector plates so that the oscillation frequency of the coil current can be adjusted to approximately four times that of the full-scale experiment. Since the skin depth is proportional to $\omega^{-1/2}$, an increase of a factor of four in the frequency scales the skin depth down by a factor of two.

The collector plates of the Langley magnetic compression experiment have been faithfully scaled in all details including the bolt holes and the slots for limiting short-circuited current. The presence of the lead bricks above the plates is simulated by a sheet-aluminum structure having the same shape as the lead bricks on the full-scale experiment. The lower lead bricks are simulated by aluminum plates bolted to the support structure. The coils and flux concentrators are constructed of aluminum, which has electrical conductivity comparable to that of the beryllium-copper theta-pinch coil. Figure 24 shows this field-shaping-experiment apparatus with a 70-centimeter-long coil made up of nine sections, each with a 5.5-centimeter bore. This figure should be compared with a similar view of the full-scale device shown in figure 10. Figure 25 shows the apparatus with the upper lead-brick simulator removed. The three variable inductors

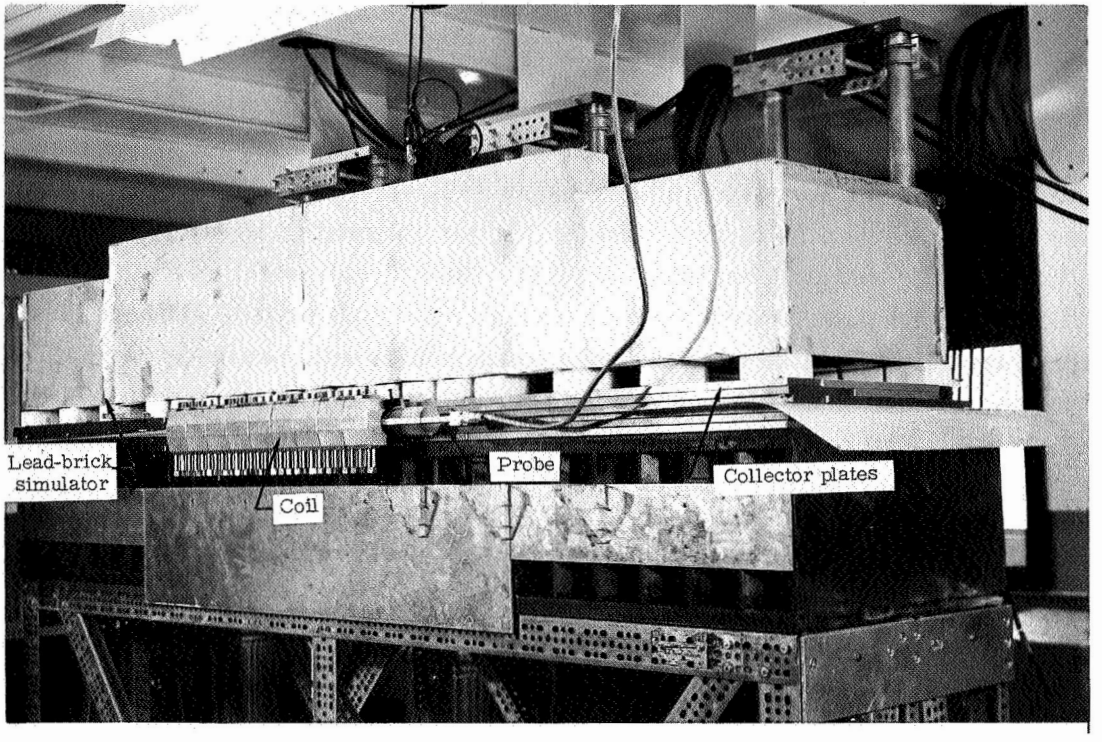

Figure 24.- The 1/2-scale model of the Langley theta pinch used for the field-shaping experiment. L-67-2086.1

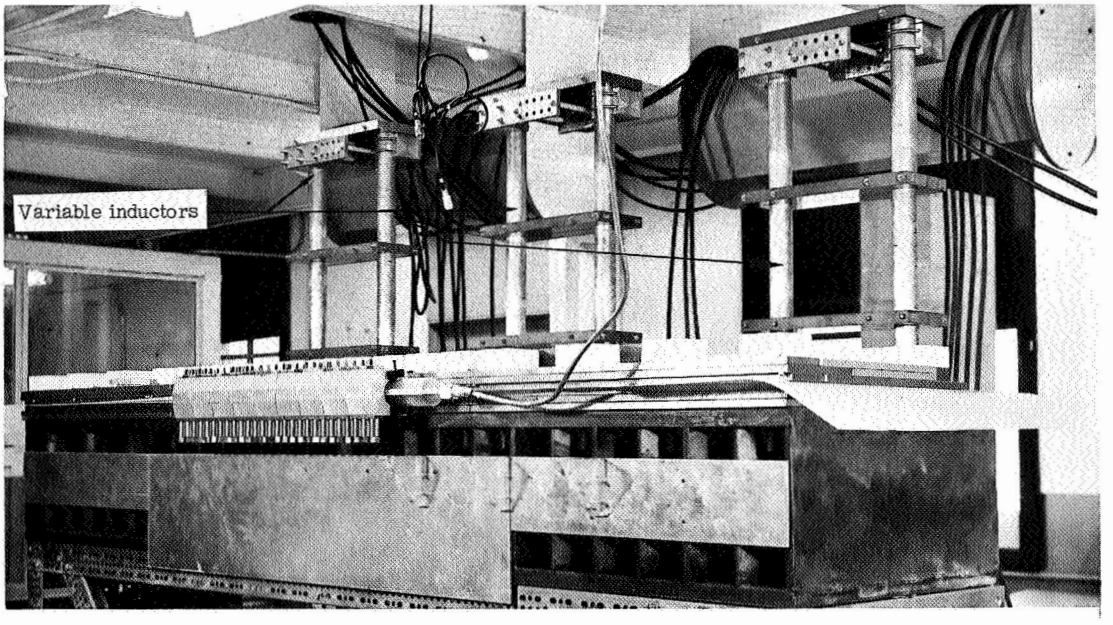

Figure 25.- Field-shaping-experiment apparatus with upper lead-brick simulator removed. L-67-2087.1

can be seen attached vertically to the back of the plates. Each inductor consists of a rectangular loop whose length may be varied. They are mounted to the collector plates by aluminum connector plates.

The power source for the field-shaping experiment is a 37.5-kilojoule capacitor bank composed of 30 1-microfarad clamshell capacitors. The capacitors are switched by modified commercial pressurized spark-gap switches. The trigger pulse for these switches is supplied by a 0.75-microfarad capacitor charged to 20 kilovolts. This capacitor in turn is triggered by a resistor-capacitor (RC) circuit which is switched by a thyratron through a 5:1 pulse transformer to give a 35-kilovolt output. The measured voltage rate of rise at the switch trigger pin as measured by a fast cathode ray oscilloscope (CRO) is greater than 1 MV/μs. This rise time insures a switch jitter of less than 20 nanoseconds. The capacitor bank is shown in figure 26. It is located on a mezzanine directly over the experiment. The current is carried by one cable per capacitor over

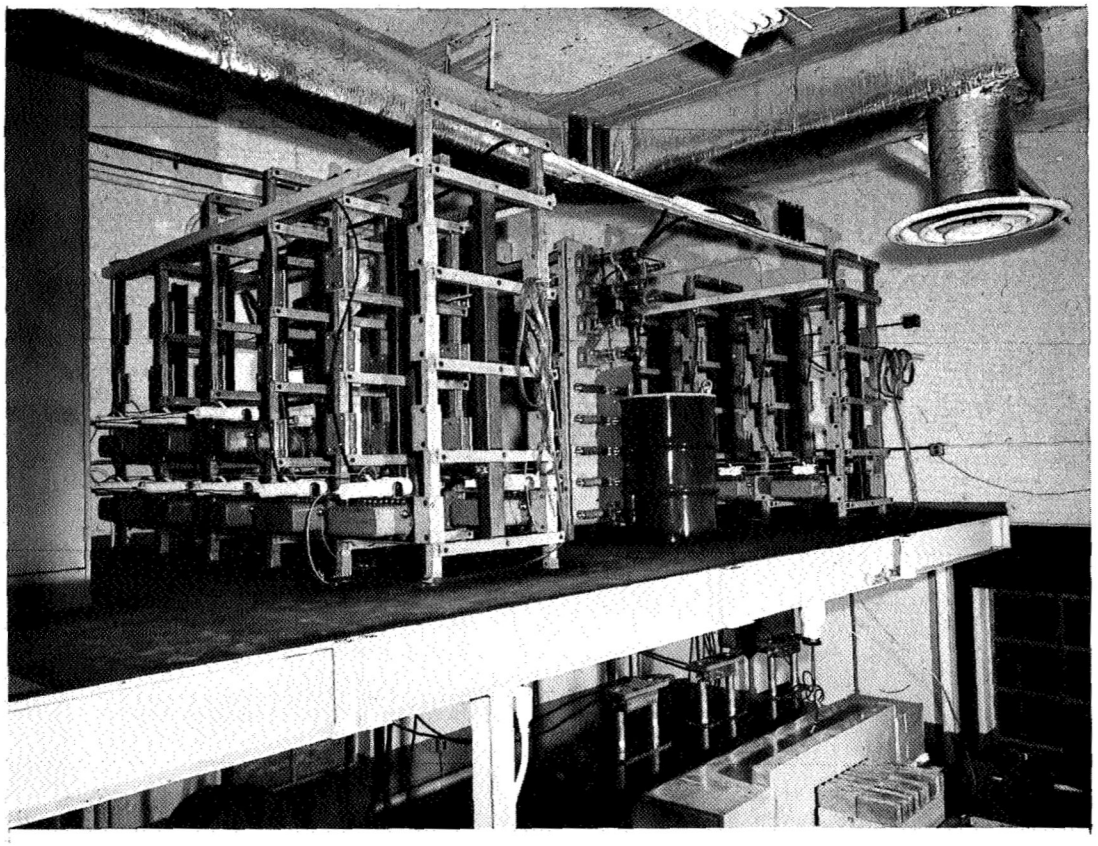

Figure 26.- Capacitor bank for the field-shaping experiment. L-67-2379

slack spools to the inductors. All cables are 5.1 meters long and have magnetically swaged terminations to reduce corona and arcing.

Initiation of the firing signal by the control system triggers the pulse generator and the CRO camera shutters which are set for a 1-second exposure. Approximately 0.5 second later the pulse generator triggers the bank and the oscilloscopes.

The voltage on the capacitor bank is monitored by an electrostatic voltmeter. By approaching the final charging voltage slowly, repeatability in bank voltage can be kept to within 0.1 percent. This accuracy has been verified by checking the repeatability of probe traces on a CRO with the use of a type-Z preamplifier to raise the scale height to 50 centimeters. In this way, changes from shot to shot of 0.1 percent could be detected.

Use of Magnetic Probes

Magnetic probes were used to measure small departures from uniformity of the magnetic field in the 1/2-scale theta pinch. In order to measure the local transverse force which would be exerted on a plasma column, one must measure the reciprocal of the local radius of curvature of field lines (see eq. (6)) given by

$$\frac{1}{R} = \frac{\nabla B}{B_Z}$$

where $\nabla B = \frac{\partial B_r}{\partial z} = \frac{\partial B_Z}{\partial r}$ since the field is curl free. Hence, a precise point-by-point measurement of B_Z and B_r would determine $1/R$. Theoretically one could just measure B_Z and determine its radial gradient; however, this process is more difficult than using measurements of B_r since the changes in B_r are comparable with B_r itself. The problem in measuring B_r is that one is attempting to measure a small field component in the presence of a large field component. This difficulty can be surmounted, however. A probe oriented to pick up B_r will generate a voltage proportional to $B_r + \alpha_1 B_Z$, where α_1 is the discrimination coefficient indicating the amount of B_Z pickup. When the probe is flipped 180^o about the Z-axis, the voltage output becomes proportional to $-B_r + \alpha_2 B_Z$, where α_2 is the discrimination coefficient. The difference in the two signals is $2B_r + (\alpha_1 - \alpha_2)B_Z$ which is equal to $2B_r$ if $\alpha_1 = \alpha_2$. The problem then is to make a probe which will maintain the discrimination coefficient α constant during the flip. Also αB_Z should be as small as possible in order to maximize the accuracy. The B_Z pickup comes from probe misalinement and (to a larger extent) from pickup in the leads. Therefore a probe was designed which would: (1) minimize stray pickup in the leads; (2) assure rigid leads so that lead loop areas would not change in the flip; (3) guarantee repeatable and accurate 180^o flips; (4) be highly precise in alinement; and (5) have high sensitivity. The five design criteria were achieved in the probe shown schematically in figure 27. Stray pickup is minimized by using an inter-8-weave cable

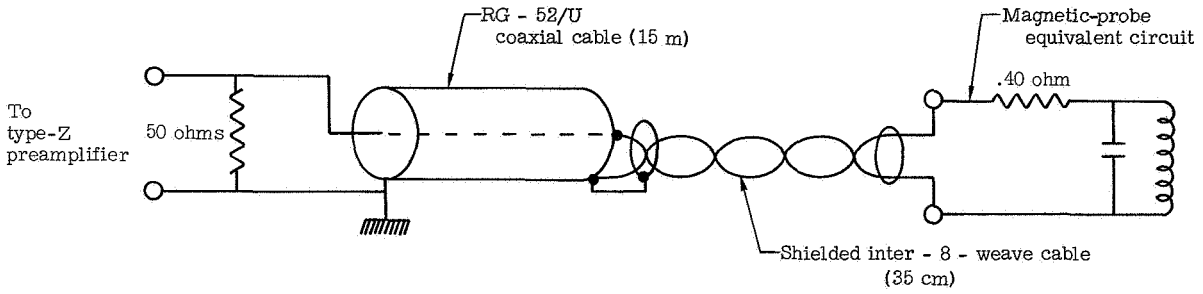

Figure 27.- Schematic diagram of magnetic probe.

with braid shielding which starts at the probe coil and continues via a copper cup and a uhf plug into the RG-52/U cable which runs to a screen room. In this way complete coaxial shielding is provided from the probe coil to the screen room and no stray loops are exposed. Additional shielding is provided by running the coaxial cable from the probe holder to the conduit in copper tubing. The leads are fixed in the teflon probe holder which has a 1-centimeter-square cross section. The probe fits in a plexiglass probe carriage which has a 1- by 4.5-centimeter slot all the way through it for the probe holder. The probe is positioned radially by 5-millimeter teflon shims. The axial location is provided in 10-centimeter steps by moving the probe carriage. Within the 10-centimeter steps, 1-centimeter increments are marked on the probe holder. This gives a radial positioning accuracy of ±0.1 millimeter and an axial positioning accuracy of ±0.2 millimeter. The square cross section and precision fit of the holder, carriage, and shims provide a precise and repeatable flip angle of 180°. The probe arrangement inserted in the theta-pinch coil is shown in figure 28. The B_r probe and a similar B_z probe are shown in figure 29. The probe coils themselves are wound on a 6-millimeter plexiglass rod, with 22 turns of enameled copper wire. The coils have a ratio of length to outer diameter of 0.72 which, according to reference 59, guarantees that the measurement is a point measurement and not an average over the fields occupying the coil volume. The coils are coated with a thin layer of polystyrene and carefully alined on the probe holder and fixed in place with a jig. The coils are then soldered to the leads and encapsulated in epoxy.

In order to test the accuracy of the probe measurements, a Helmholtz coil was constructed (see fig. 30). The Helmholtz coil, in principle, will produce a magnetic field whose line curvatures can be precisely calculated. The problem is that deviation of the

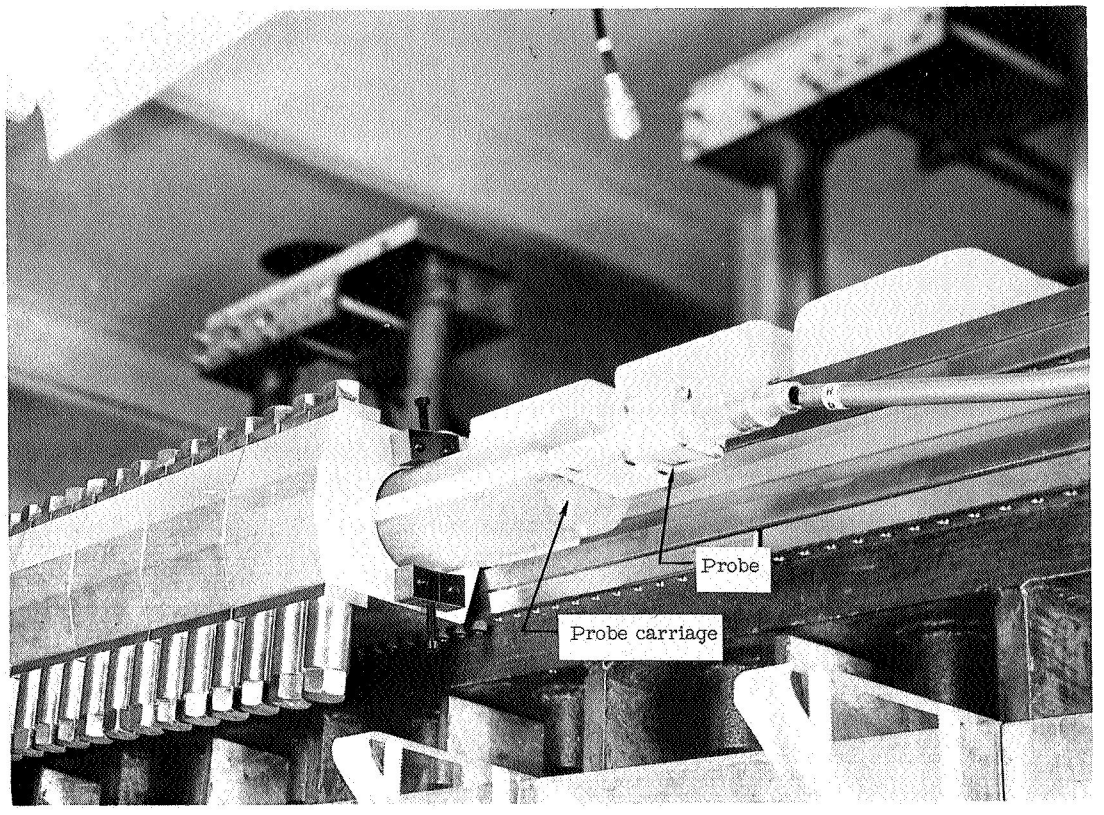

Figure 28.- Probe inserted in theta-pinch coil. L-67-2085.1

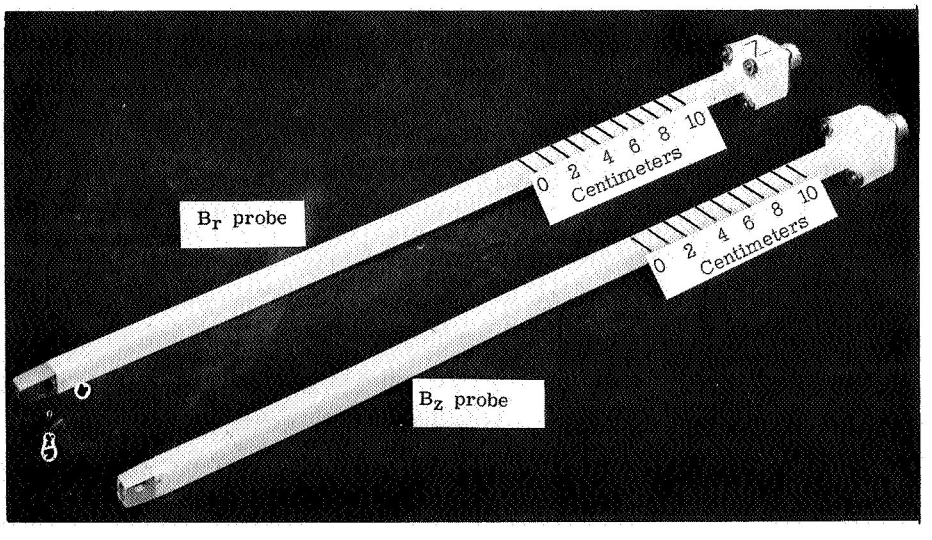

Figure 29.- The B_r and B_z probes. L-67-2376.1

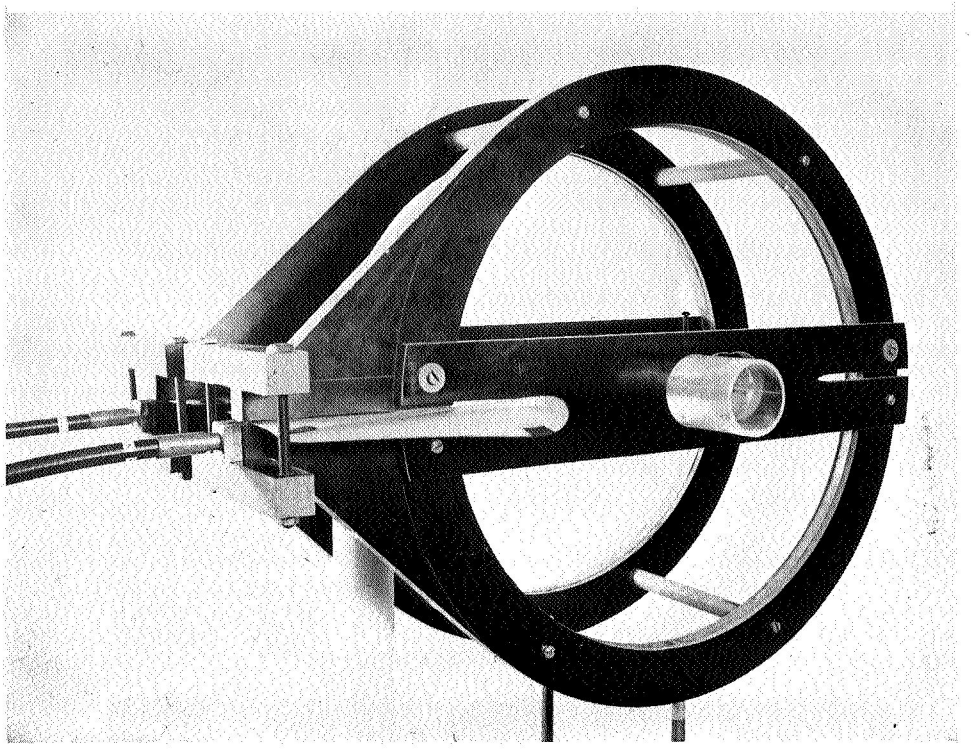

Figure 30.- The Helmholtz coil. L-67-2377

field from perfection by, say, one part in a hundred due to disturbances from the leads is hard to avoid. This situation was shown to exist when a measurement of B_r at the geometrical center of the coil, where B_r should ideally be zero, showed that a value for B_r of 1.28 percent of B_z existed. Effort was made to reduce this interference, without appreciable improvement. The basic problem seems to be that the Helmholtz coil has a single turn. A multiturn coil would suffer less from lead interference; however, its construction for high-voltage operation would be rather elaborate. Consequently, measurements of B_r were made in the imperfect Helmholtz coil along an axis 5 centimeters offcenter, from the median plane ($z = 0$) outward to the plane of one coil ($z = 12$ cm). These measurements are shown in figure 31. The height of the error bars is determined by the signal-to-noise ratio of the oscillograms. A curve was fitted to the points and then differentiated so that the field-line curvatures could be determined. Measured values of radius of curvature are compared with values calculated for an ideal Helmholtz coil in figure 32. The close fit of the points to a smooth curve and the detection of the small effect of negative curvature close to the median plane were highly encouraging.

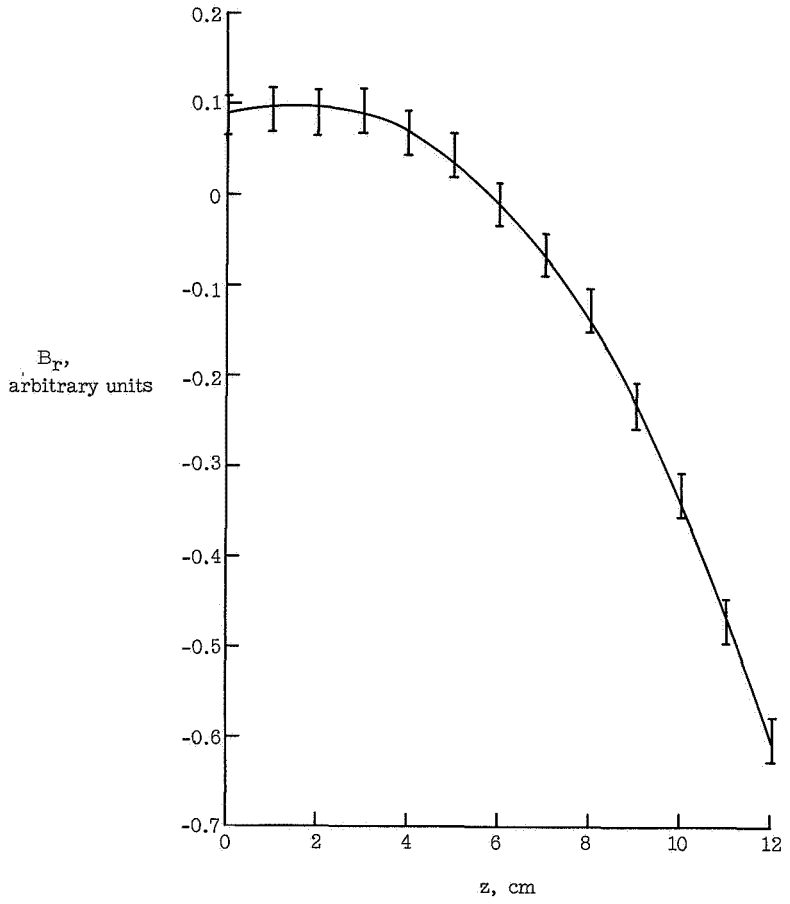

Figure 31.- Measurements of B_r in Helmholtz coil at r = 5 centimeters.

Measurements of B_r were made in the following six 1/2-scale theta-pinch configurations:

(1) Configuration with normal coil and with lead-brick simulators but without extension (see fig. 24);

(2) Configuration (1) with upper lead-brick simulator removed (see fig. 25);

(3) Configuration with flux-concentrator coil and with lead-brick simulators but without extension;

(4) Configuration (3) with upper lead-brick simulator removed;

(5) Configuration with normal coil, with extension, and with lead-brick simulators placed 15.24 centimeters above extension to top collector plate; and

(6) Configuration with flux-concentrator coil, with extension, and with lead-brick simulators placed 15.24 centimeters above extension to top collector plate (see fig. 33).

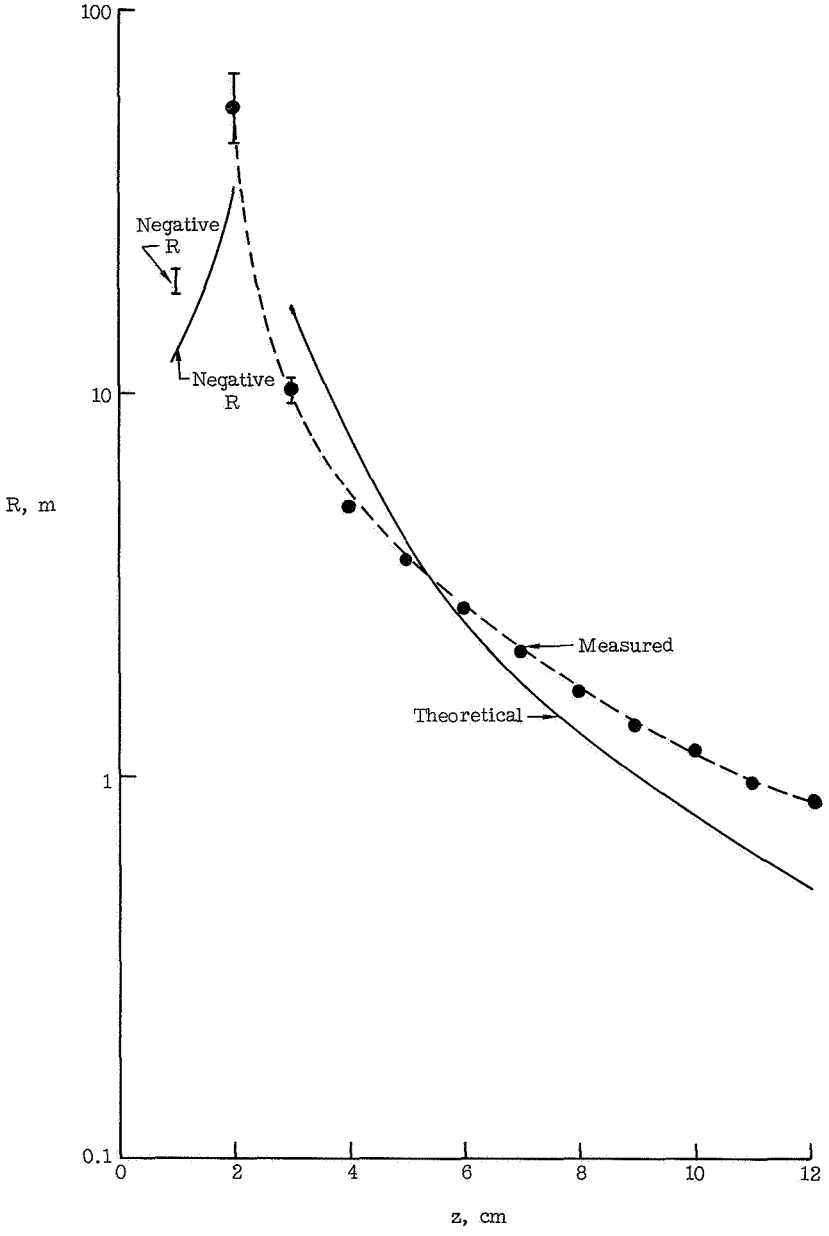

Figure 32.- Curvature measurements in Helmholtz coil of radius 22.5 centimeters at r = 5 centimeters compared with calculated values.

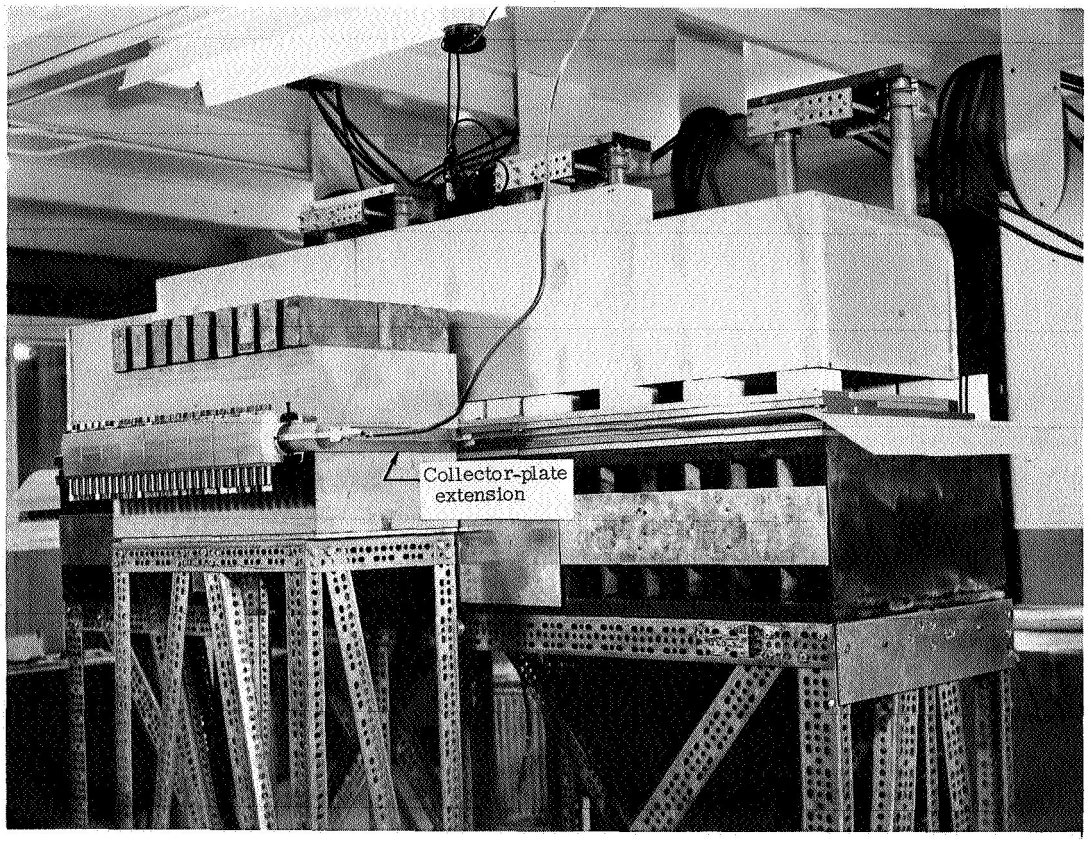

L-67-2375.1

Figure 33.- The 1/2-scale model of the Langley theta pinch with extension and flux concentrator.

The extension has a width equal to the coil length (70 centimeters) and places the coil 40.5 centimeters forward. The extension to the top collector plate is laminated into nine sections, each having the same width as the coil sections, with a 1.5-millimeter gap between them. The current flow in the extension to the bottom plate, even though it is unlaminated, follows the flow pattern in the extension to the top plate because of the skin effect. Hence, the effective length-width ratio of the extension is 5.4.

The flux-concentrator coil is shown partially assembled in figure 34. The flux concentrator is a bored-out version of the normal coil such that the bore of the flux concentrator, which has a wall thickness of 6.35 millimeters, is the same as the bore of the normal coil (5.5 centimeters). The concentrator and coil are machined from solid aluminum.

For experimental measurement of the radial magnetic field in these six configurations, it was found that the signal-to-noise ratio could be optimized by reducing the capacitance of the bank to 6 microfarads and operating with a charging voltage of 10 kilovolts. In order to maintain the frequency as near 80 kilocycles as possible (for purposes

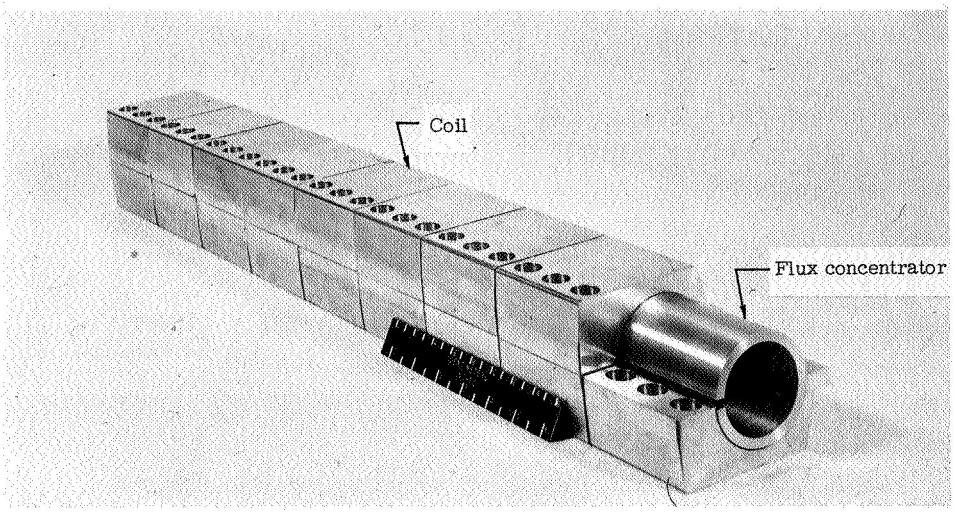

Figure 34.- The flux-concentrator coil. L-67-2088.1

of scaling the skin depth), the inductors had to be tuned for maximum inductance. The result was an operating frequency of 96.7 kilocycles. The voltage on the bank appeared almost entirely across the inductors; only 250 volts were applied to the coil and thus the insulation problem was greatly simplified.

Measurements of B_r were made 7.5 and 17.5 millimeters offcenter radially in each direction in the plane of the coil feed slot. The radial direction toward the collector plate is taken as negative; the direction away from the coil slot is taken as positive. Measurements are made at intervals of 3 centimeters along the coil axis starting with $z = 0$ at the median plane and progressing to $z = 30$ centimeters, which is 5 centimeters from the end of the coil. The signals are carried to the screen room by a RG-52/U coaxial cable and terminated with 50 ohms. A type-Z preamplifier with a CRO was used and the oscillograms were recorded photographically by an electrically actuated camera. The preamplifier features a dc bias voltage which can be used to raise the scale height and allow high gain to be used for maximum reading accuracy. This bias voltage was employed to give the signals a scale height of 6 centimeters whenever possible. The results of these measurements are presented in the following section.

RESULTS AND DISCUSSION

Field-Shaping-Experiment Results

The results of the measurements of B_r in the field-shaping experiment are shown in figure 35.

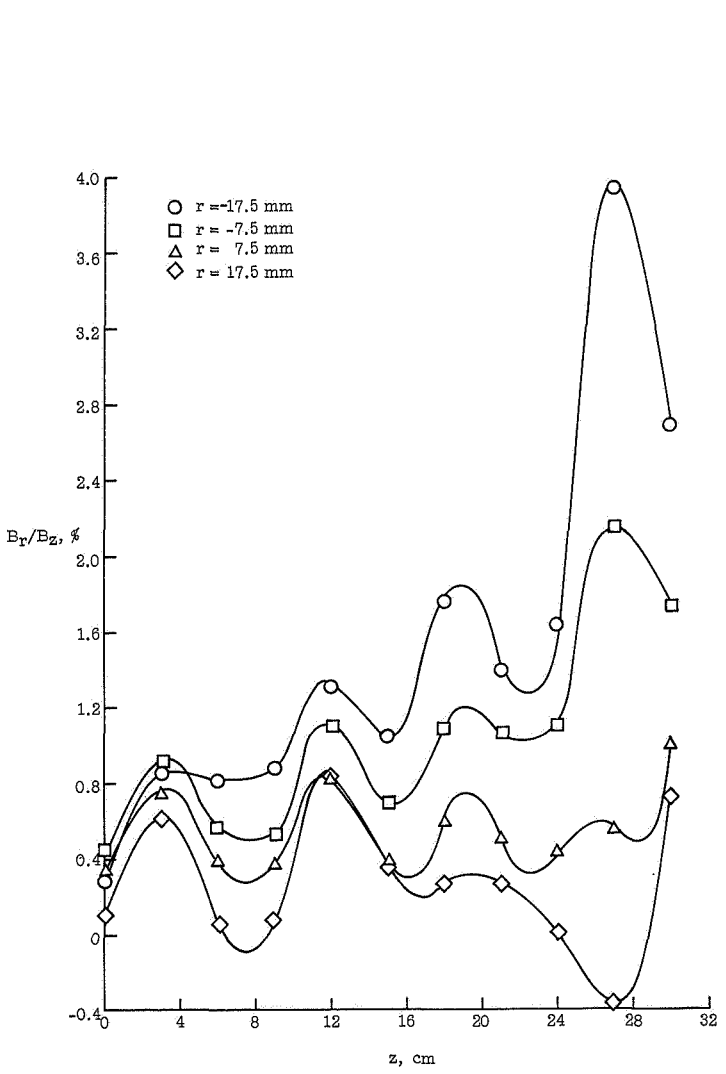

(a) Configuration with normal coil and with lead-brick simulators but without extension (see fig. 24).

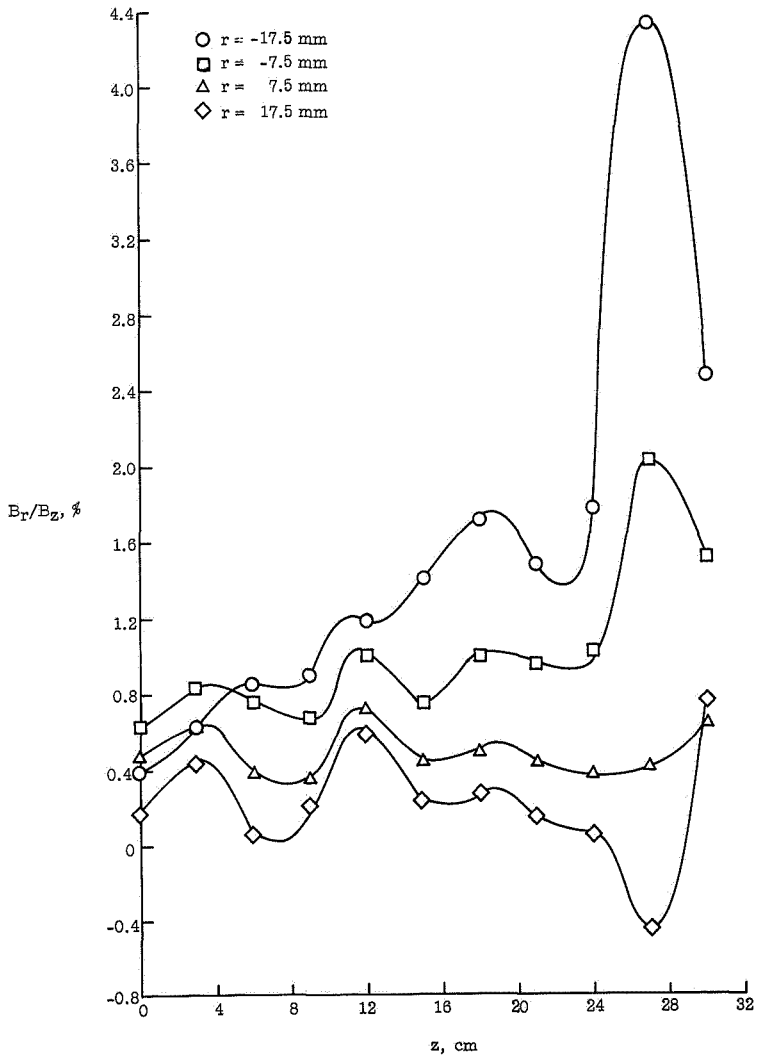

(b) Configuration with normal coil and with lower lead-brick simulator but without upper lead-brick simulator or extension (see fig. 25).

Figure 35.- Measurements of B_r taken at four radial positions for various field-shaping-experiment configurations.

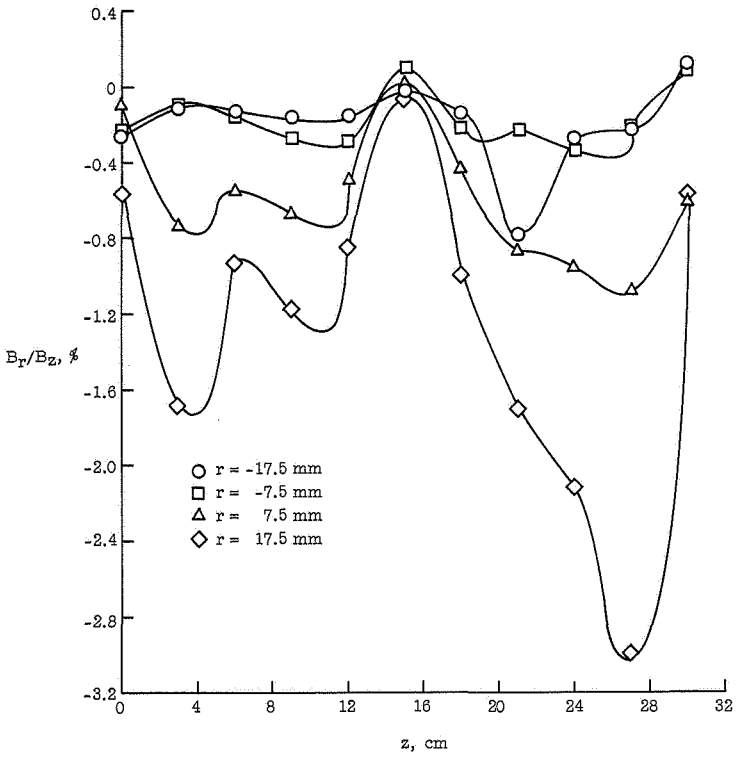

(c) Configuration with flux-concentrator coil and with lead-brick simulators but without extension; flux concentrator has a 1-centimeter slot.

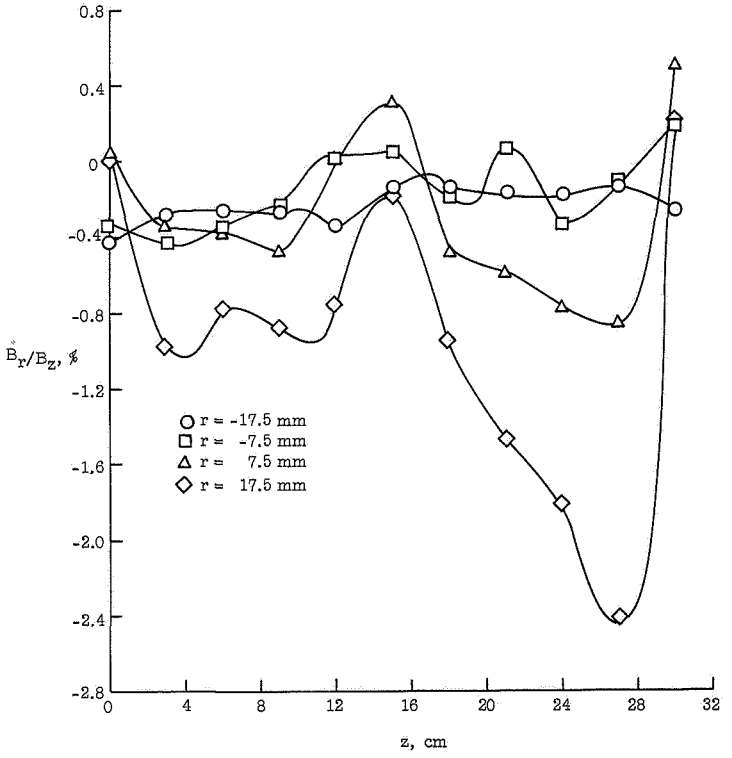

(d) Configuration with flux-concentrator coil and with lower lead-brick simulator but without upper lead-brick simulator or extension; flux concentrator has a 1-centimeter slot.

Figure 35.- Continued.

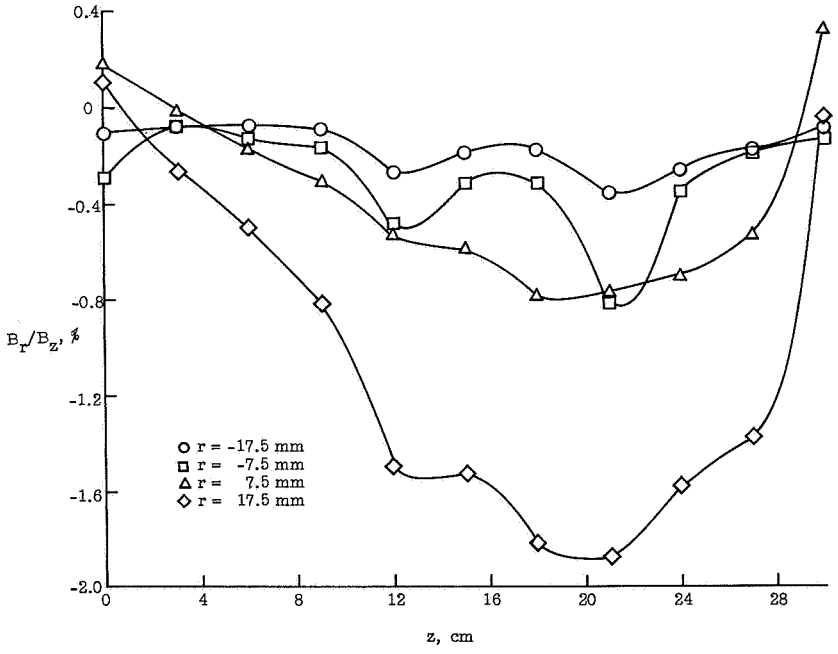

(e) Configuration with flux-concentrator coil and with lead-brick simulators but without extension; flux concentrator has a 0.25-millimeter slot (oriented as shown in fig. 22).

Figure 35.- Continued.

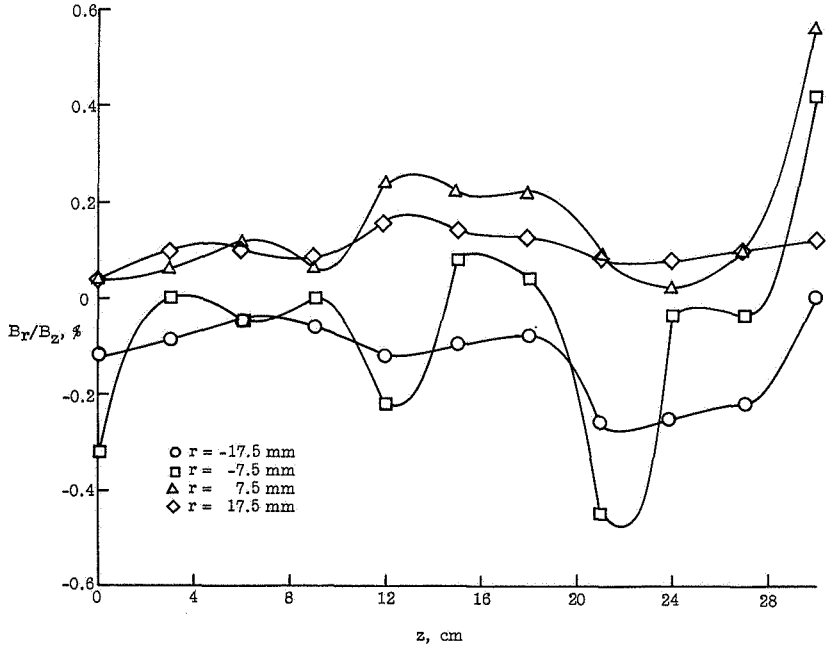

(f) Configuration with flux-concentrator coil and with lead-brick simulators but without extension; flux concentrator has a vertically oriented 0.25-millimeter slot.

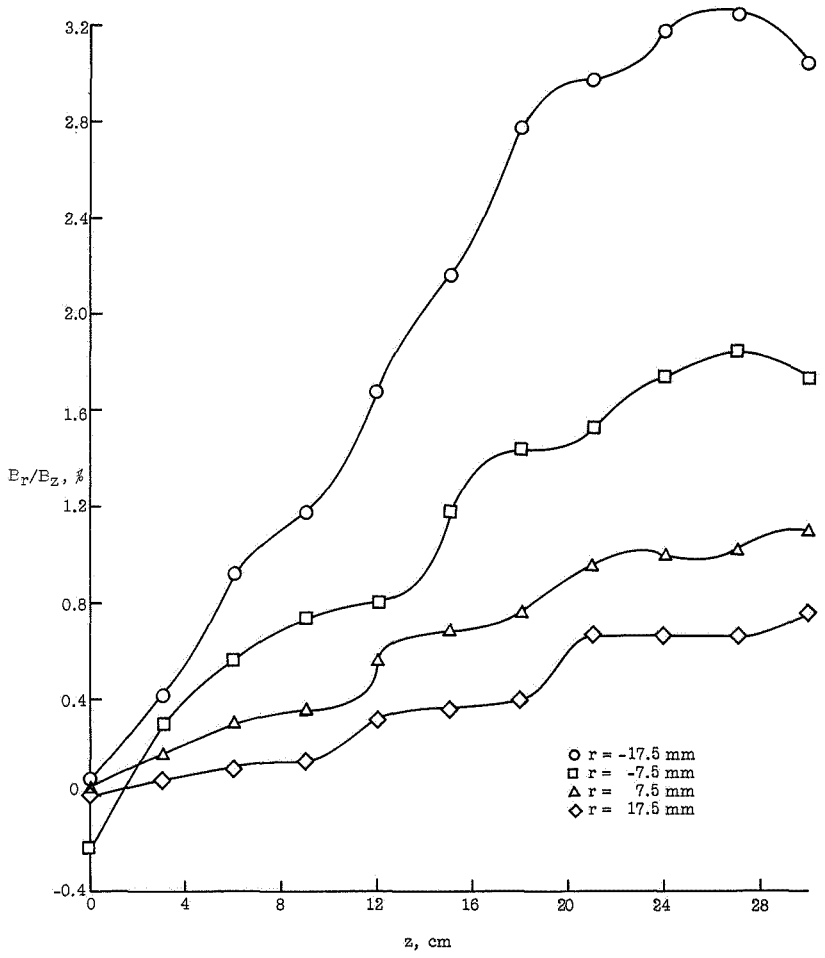

(g) Configuration with flux-concentrator coil and with lead-brick simulators but without extension; flux concentrator has a 0.25-millimeter slot alined with the coil feed slot.

Figure 35.- Continued.

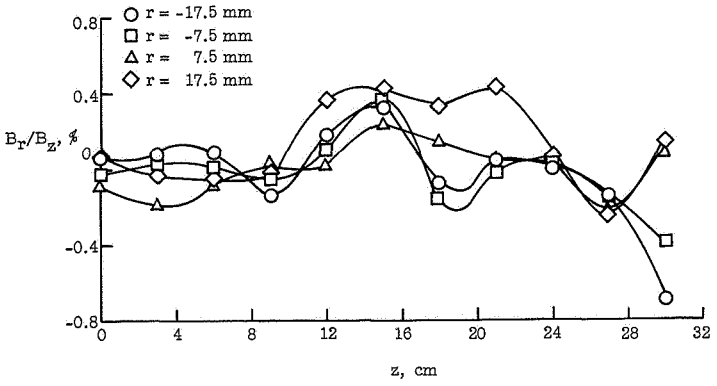

(h) Configuration with normal coil and extension.

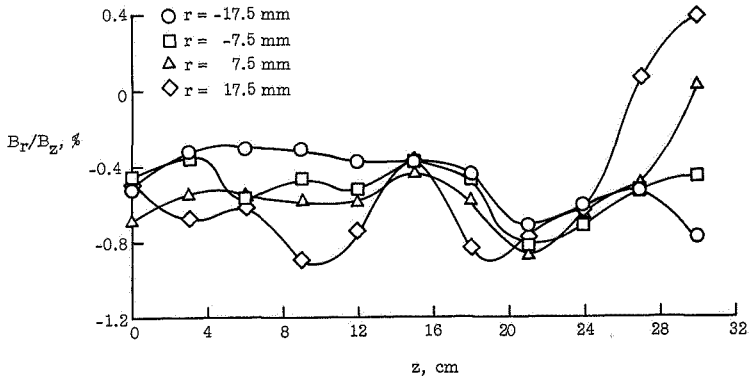

(i) Configuration with flux-concentrator coil and extension; flux concentrator has a 1-centimeter slot.

Figure 35.- Concluded.

In figure 35(a) the gradient in B_r is seen to diminish as the measurement location is moved away from the coil feed slot. This is essentially the same result found in reference 4 for a 1/5-scale model. Ripples are observed in the B_r/B_z curve, the peaks of which correspond to the vertical slots between coil sections. The source of these ripples becomes evident upon inspecting figure 35(b), which shows results for a configuration that differs from the configuration considered in figure 35(a) only in that the upper lead-brick simulator has been removed. The amplitude of the ripples has been somewhat reduced although the character of the curves is the same. This effect is due to currents set up in the collector-plate structure.

Figures 35(c) and 35(d) show the B_r field inside the flux concentrator with and without the presence of the upper lead-brick simulator, respectively. Again, although the character of the curves is clearly the same, the ripple amplitude is somewhat less when the upper simulator is not present. Note that the more irregular field is on the positive side of the coil center line and that the field nearest the collector plate is quite smooth. Most important, the insertion of the flux concentrator has almost eliminated net field curvature. The effect of the ripples on the plasma is impossible to predict exactly, although it may well be that alternate regions of opposite curvature tend to inhibit instabilities by shorting out the charge separations which drive them.

On the assumption that the rather irregular field near the flux-concentrator slot was caused by the large width of the slot (1 centimeter), a new flux concentrator was machined with a 0.25-millimeter slot and the experiment was rerun. The results are shown in figure 35(e). The amplitude of B_r is reduced by approximately one-third and the variation of B_r with axial distance close to the flux-concentrator slot simply suggests that some flux is lost as a result of smooth bending of field lines into the slot. These effects were confirmed by rotating the narrow-slot flux concentrator 90^o such that the slot was vertical. The data taken for this configuration are shown in figure 35(f). This figure shows a very uniform field with an average amplitude for B_r of less than 0.1 percent of B_z and no net gradient. In order to confirm the original concept of the flux concentration, the slot was next alined with the coil feed slot and measurements were made. It was anticipated that the result would be just as though no flux concentrator were present except that the ripples seen in figure 35(a), which were shown to correlate with the gaps between coil sections, would be absent. Figure 35(g) shows that the data obtained with the slots alined conform to the expected result.

Figures 35(h) and 35(i) show the results for a collector-plate extension. These data reveal a highly uniform magnetic field and support the prior supposition that the current funneling is a dominating effect. It is interesting to note that the current-transfer effect (see section "Coil-Collector Discontinuity"), which was masked in figures 35(a) to 35(e)

and in figure 35(g) by either ripple or current funneling, is now in evidence. In figure 35(i), for which the wide-slot flux concentrator is used, the field nearest the concentrator slot (r = 17.5 mm) has a positive gradient. These effects are small and somewhat localized and would probably not limit the plasma containment time.

As seen from equation (6), the transverse force which causes plasma drift is proportional to $1/R$, where R is the radius of curvature of the field lines. An average radius of curvature for each of the four radial positions in the six configurations has been calculated by considering values of B_r only at $z = 0$ and $z = 30$. It is likely that the average curvature is the most influential factor in the drift characteristics of the plasma column. These average radii of curvature have been scaled up to apply to the full-scale Langley theta pinch (i.e., coil length of 140 centimeters and coil bore of 11 centimeters). The reciprocal of the radius of curvature $1/R$ is plotted as a function of radial position in figures 36, 37, 38, and 39, which show, respectively, the extension effect, the flux-concentrator effect, the lead-brick effect, and the extended-flux-concentrator effect. The direction of the forces is indicated by arrows on the data points. The selection of the end point at 30 centimeters for use in determining the gradient may be justified somewhat by the fact that it is neither in line with the vertical slot nor in the extreme end region where the field has begun to flare. The choice still has a certain arbitrariness about it, however, and this, as well as the averaging of $1/R$ over z, must be weighed in evaluating the curves in figures 36 to 39.

First, the effect of the extension is considered. A comparison is made between the scaled-up results for the normal coil without the extension (both with and without the upper lead-brick simulator present) and the scaled-up results for the normal coil on the extension. Figure 36 shows that the forces exerted when the extension is used are smaller than when it isn't. Moreover, the transfer effect causes the drift forces that do exist when the extension is used to be always directed toward the center of the coil rather than toward the wall. Therefore the extension should certainly suffice to stabilize the plasma column against drift.

The flux-concentrator effect is shown next in a comparison of the scaled-up results for the flux-concentrator and normal coils both with and without the upper lead-brick simulator present. The arbitrariness of the method by which the curves in figure 37 were obtained may have resulted in somewhat inconclusive results. The fact that the flux-concentrator radial field has such a large ripple makes the average curvature somewhat more uncertain than in the normal-coil cases. It would seem, however, that the average curvature is less for the flux-concentrator coil than for the corresponding normal coil.

Unfortunately, the results are also inconclusive in evaluating the effect of the lead-brick simulator on the average curvature. The lead-brick-simulator effect is shown in

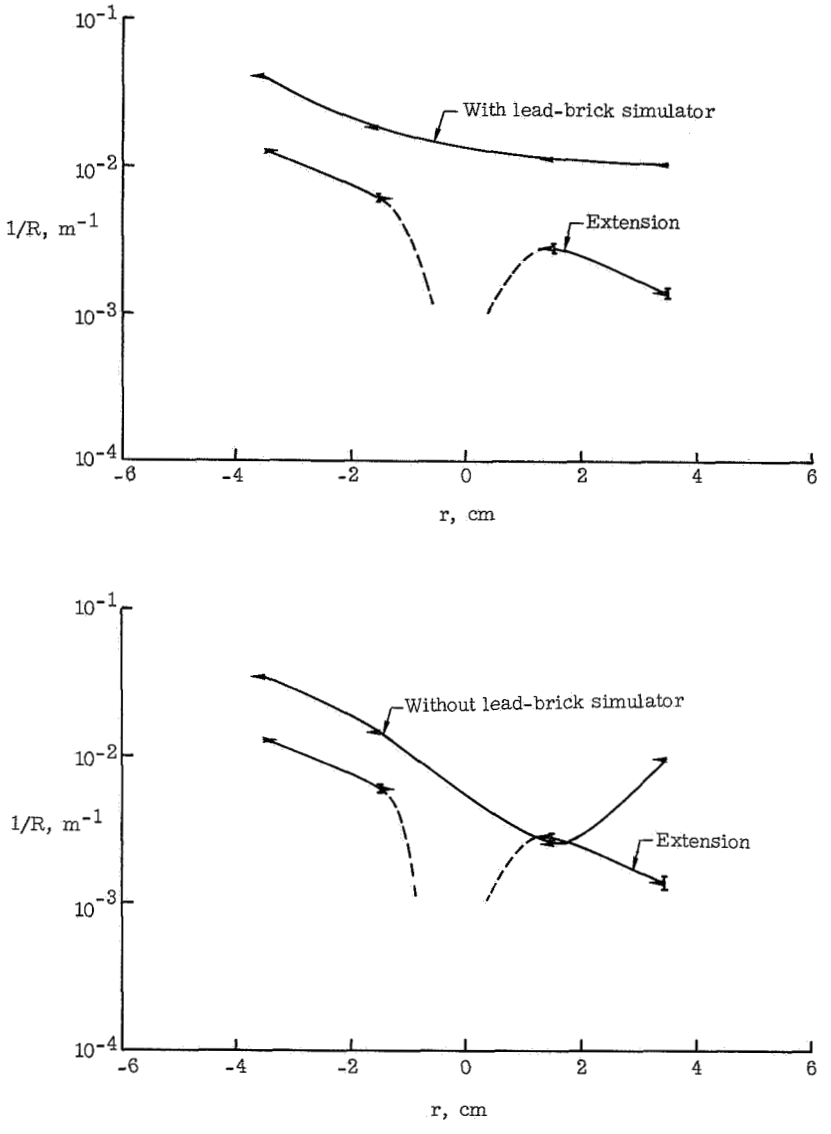

Figure 36.- The extension effect, as shown by a comparison between the scaled-up results for the normal coil without the extension (both with and without the upper lead-brick simulator present) and the scaled-up results for the normal coil with the extension.

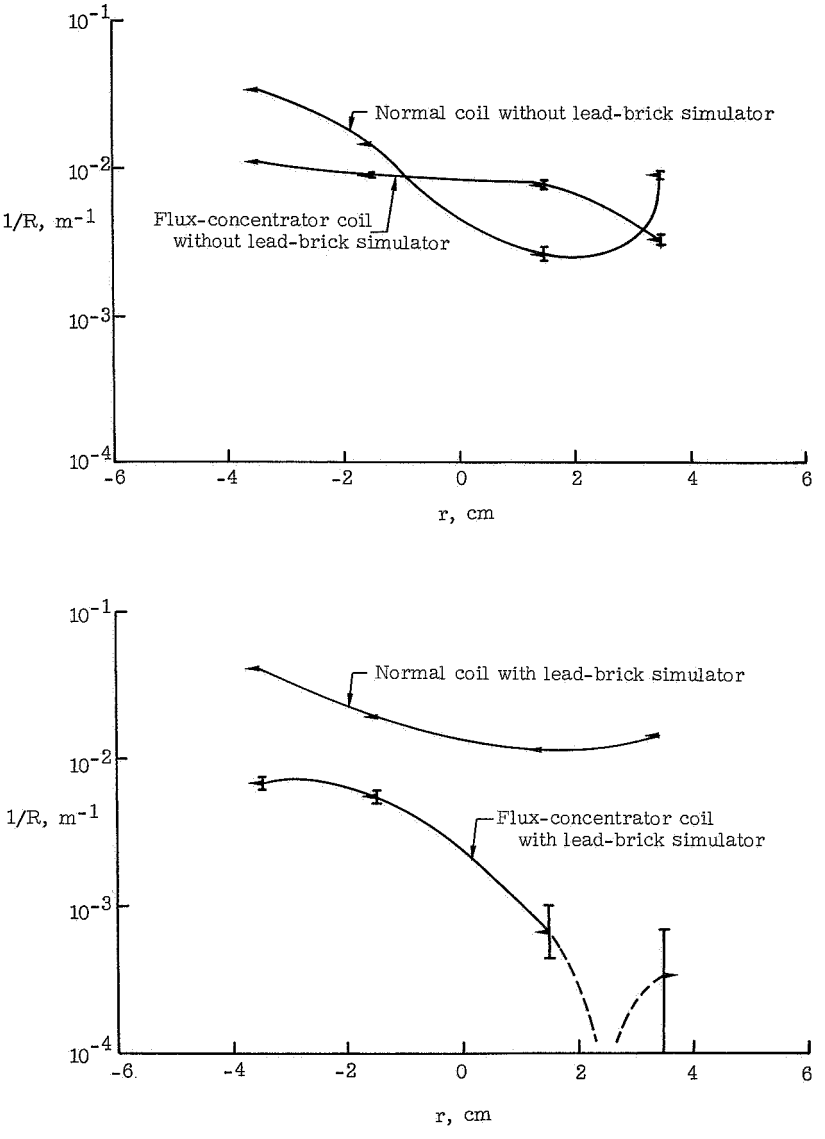

Figure 37.- The flux-concentrator effect, as shown by a comparison of the scaled-up results for the flux-concentrator and normal coils both with and without the upper lead-brick simulator present.

figure 38. For the normal coil the removal of the simulator appears to give a slight reduction in the drift forces, whereas for the flux-concentrator coil the presence of the simulator seems beneficial. In general, the previously stated conclusion, that the main effect of the large conducting mass on one side of the coil seems to be the introduction of ripple into the field, must stand as the only result which can be observed.

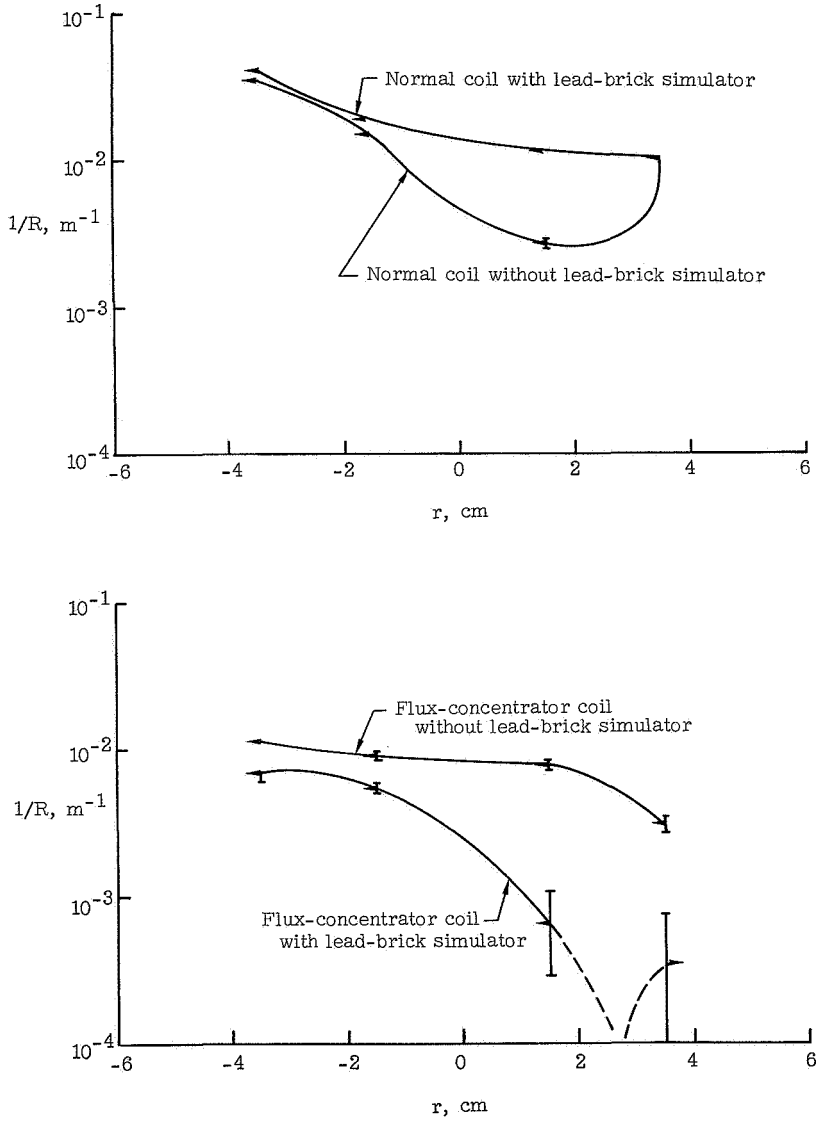

Figure 38.- The lead-brick effect, as shown by a comparison of the scaled-up results for the presence and absence of the upper lead-brick simulator for both the normal and flux-concentrator coils.

The effect of an extended flux concentrator on the curvature is shown in figure 39. The average forces seem to be about the same for the normal coil on the extension and the flux-concentrator coil on the extension. The previously mentioned effect of the current transfer can be seen on both curves.

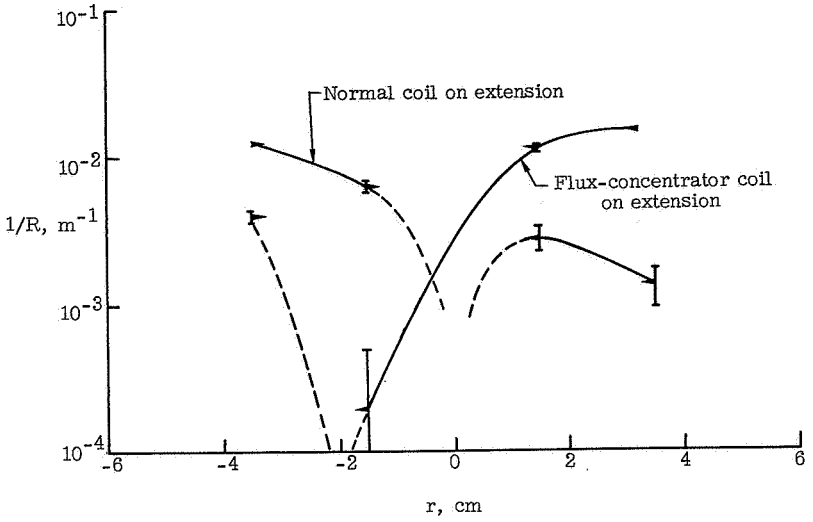

Figure 39.- The effect of the extended flux concentrator, as shown by a comparison between the scaled-up results obtained with the normal coil on the extension and the scaled-up results obtained with the flux-concentrator coil on the extension.

Stabilizing Effect of Flux Concentrator on Drift in Full-Scale Theta Pinch

Preliminary tests have been performed on the Langley theta pinch to determine the effect of a flux concentrator on the plasma drift. The flux concentrator used consisted of two pieces, with the center slot in an eight-section coil being left uncovered. The concentrator was rolled from a 1.6-millimeter-thick copper sheet, with a 25-millimeter slot being left between the two pieces, and was insulated by poly[ethylene terephthalate] plastic film from the coil.

Drift data were obtained with the slot of the flux concentrator on the same side of the coil as the current-feed slot and also with the flux concentrator rotated 180°. The results are compared in figure 40. In addition to streak photography of the plasma column by an image-converter camera, the intensity of strong lines of Si III at 3090 Å was monitored photoelectrically side-on by a monochromator. The sweep duration of the streak camera was 50 μs. The filling pressure of the hydrogen in the tube was 100 millitorr and the bank was operated at a charging voltage of 10 kilovolts to give an energy of 250 kilojoules.

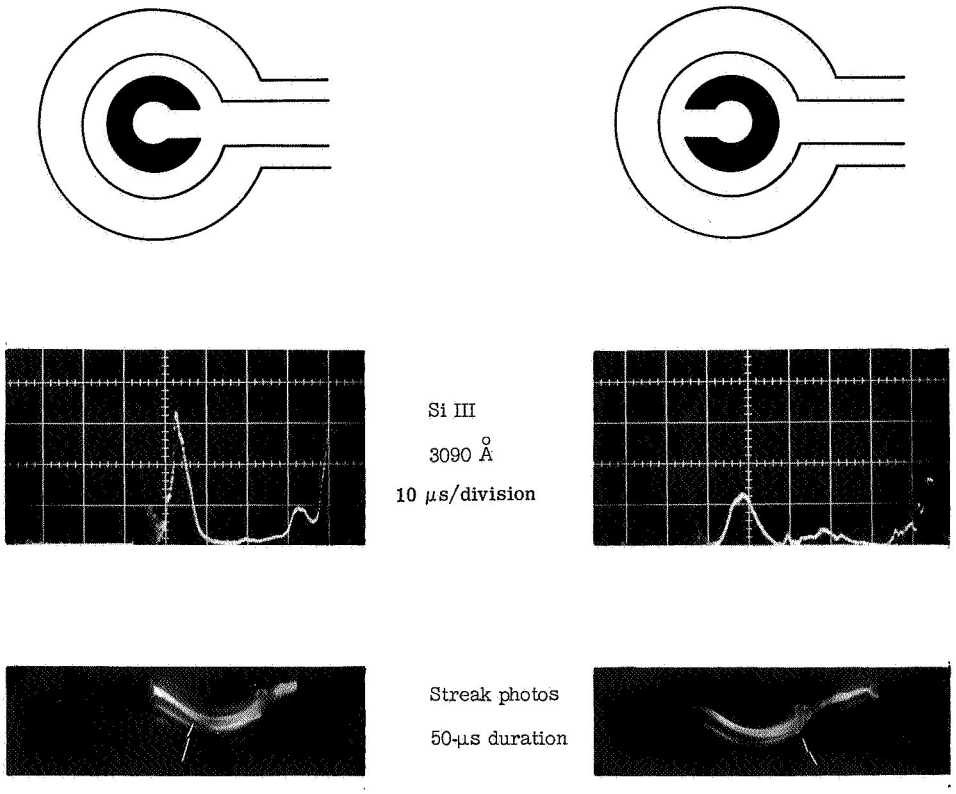

L-68-10,079

Figure 40.- Drift control by flux concentrator. (The points on the streak photographs where the plasma strikes the tube wall are indicated by arrows.)

One sees from the streak photograph on the left-hand side of figure 40 that the plasma struck the wall shortly before maximum current. This correlation is easily made as a result of the distortion in the image-converter tube optics produced by the field. Note also that the Si III signal rises strongly after 8 μs. The right-hand side of the figure is for the flux concentrator oriented to stabilize the drift. The filling pressure and bank energy are identical to those used for the flux concentrator having its slot alined with the coil slot. The Si III signal remains small during the whole test and the streak photograph shows a reasonably well-centered plasma column with only a slight suggestion of interaction with the inside wall near the end of the half-cycle of coil current. Unfortunately these results did not prove to be indefinitely repeatable. The stabilizing effect seemed to decay as additional shots were taken. Some of these shots, taken with the flux concentrator in the stabilizing position, are shown in figure 41 in chronological order. Progressive contamination of the tube wall may have been responsible for the breakdown of the stabilizing effect. Further work done on the plasma purity problem since these tests were made seems to bear out this hypothesis.

It has been established that a definite correlation exists between pump-out time (a good indicator of the general cleanliness of the system) and the ability to produce a quiescent reproducible plasma. At the time the tests were made, considerable

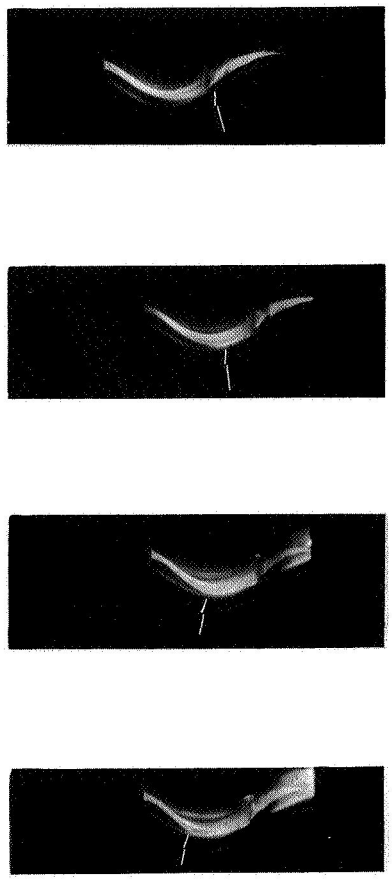

L-68-10,080

Figure 41.- Decay of the flux-concentrator stabilizing effect probably due to progressive wall contamination, as shown by streak photographs of 50-μs duration. (These photographs are presented in chronological order, with the one taken earliest at the top, and represent the trend through 20 shots; the points where the plasma strikes the tube wall are indicated by arrows.)

contamination existed and it is probable that axial motion in the turbulent plasma may have given rise to the decay of the drift stabilization as the contamination increased from shot to shot.

CONCLUSIONS

Arguments have been advanced to suggest that the major cause of drift in a theta-pinch plasma is magnetic-field-line curvature due mainly to the funneling of current from a long collector plate into a short coil. The rotational instability also seems to be influenced by magnetic-field uniformity although the exact mechanism is no doubt complex.

Magnetic-probe measurements have been made to ascertain the magnitude of the effect of the large conducting collector-plate structure, a collector-plate extension, and a flux concentrator on the vacuum-field structure in the coil. The flux-concentrator technique investigated by the author has been shown to reduce the field-line curvature, and tests performed on the full-scale theta pinch have suggested that a simple flux concentrator is capable of stabilizing the drift.

Langley Research Center,
National Aeronautics and Space Administration,
Langley Station, Hampton, Va., September 23, 1968,
129-02-01-02-23.

REFERENCES

1. Quinn, Warren E.: Studies of Plasmas in Fast Magnetic Compression Experiments. Plasma Physics and Thermonuclear Research, vol. 2, C. L. Longmire, James L. Tuck, and W. B. Thompson, eds., Macmillan Co., 1963, pp. 150-188.

2. Reynolds, J. A.; Aldridge, E. E.; Keilhacker, M.; and Niblett, G. B. F.: Control of Plasma Drift in the Thetatron. Phys. Fluids, vol. 8, no. 3, Mar. 1965, pp. 529-538.

3. Thonemann, Peter C.; and Kolb, Alan C.: Plasma Rotation and Instability in the θ-Pinch Due to Transverse Magnetic Fields. Phys. Fluids, vol. 7, no. 9, Sept. 1964, pp. 1455-1461.

4. Hintz, E.; Kolb, A. C.; Lupton, W. H.; and Griem, H. R.: Drift of a θ Pinch in a Ioffe Multipole Field. Phys. Fluids (Res. Notes), vol. 7, no. 1, Jan. 1964, pp. 153-154.

5. Kolb, Alan C.: Magnetic Compression of Plasmas. Rev. Mod. Phys., vol. 32, no. 4, Oct. 1960, pp. 748-756.

6. Jeans, James: An Introduction to the Kinetic Theory of Gases. Cambridge Univ. Press, 1960.

7. Sato, Masatomo: Stability of Plasma, I. IPPJ-7, Nagoya Univ. Inst. Plasma Phys., Mar. 1963.

8. Bodin, H. A. B.; Green, T. S.; Niblett, G. B. F.; Peacock, N. J.; Quinn, J. M. P.; and Reynolds, J. A.: The Influence of Trapped Field on the Characteristics of a Magnetically Compressed Plasma (Thetatron). Nucl. Fusion, 1962 Suppl. – pt. 2, pp. 521-532.

9. Little, E. M.; Quinn, W. E.; Ribe, F. L.; and Sawyer, G. A.: Studies of Stability and Heating in the Scylla Magnetic Compression Experiment. Nucl. Fusion, 1962 Suppl. – pt. 2, pp. 497-509.

10. Griem, H. R.; Kolb, A. C.; Lupton, W. H.; and Phillips, D. T.: Measurements of Electron Densities and Temperatures and Other Plasma Parameters in Magnetic Compression Experiments. Nucl. Fusion, 1962 Suppl. – pt. 2, pp. 543-551.

11. Bodin, H. A. B.; and Newton, A. A.: Rotational Instability in the Theta Pinch. Phys. Fluids, vol. 6, no. 9, Sept. 1963, pp. 1338-1345.

12. Kruskal, M.; and Schwarzschild, M.: Some Instabilities of a Completely Ionized Plasma. Proc. Roy. Soc. (London), ser. A, vol. 223, May 6, 1954, pp. 348-360.

13. Lehnert, B.: Stability of a Plasma Boundary in a Magnetic Field. Phys. Fluids, vol. 4, no. 7, July 1961, pp. 847-854.

14. Lehnert, B.: Plasma Stability in an Inhomogeneous Magnetic Field. Phys. Fluids, vol. 5, no. 4, Apr. 1962, pp. 432-438.

15. Rosenbluth, M. N.; Krall, N. A.; and Rostoker, N.: Finite Larmor Radius Stabilization of "Weakly" Unstable Confined Plasmas. Nucl. Fusion, 1962 Suppl. – pt. 1, pp. 143-150.

16. Schmidt, George: Physics of High Temperature Plasmas. Academic Press, Inc., 1966.

17. Rostoker, Norman; and Kolb, Alan C.: Fission of a Hot Plasma. Phys. Rev., Second ser., vol. 124, no. 4, Nov. 15, 1961, pp. 965-969.

18. Kvartskhava, I. F.; Kervalidze, K. N.; Zukakishvili, G. G.; and Gvaladze, Yu. S.: Experiment on the Use of an Auxiliary Discharge to Investigate Plasma Properties in a Theta Pinch With a Trapped Reverse Magnetic Field. Nucl. Fusion, vol. 3, no. 4, Dec. 1963, pp. 285-292.

19. Keilhacker, M.; Herold, H.; Cooper, J.; and Roberts, D. E.: Doppler Shift Measurements to Investigate Plasma Rotation in the Theta Pinch. Plasma Physics and Controlled Nuclear Fusion Research, Vol. I., Int. At. Energy Agency, 1966, pp. 315-330.

20. Haines, M. G.: On the Origin of Rotation in Magnetically Confined Plasmas. Advan. Phys., vol. 14, no. 54, Apr. 1965, pp. 167-211.

21. Rostoker, Norman; and Kolb, Alan C.: Rotations of Plasmas in θ Pinches. Phys. Fluids (Comments), vol. 5, no. 6, June 1962, pp. 741-742.

22. Taylor, J. B.: Rotation and Instability of Plasma in Fast B_Z Compression Experiments. J. Nucl. Energy: Pt. C, vol. 4, no. 6, Dec. 1962, pp. 401-407.

23. Jensen, T. H.; and Voorhies, H. G.: On Angular Momentum of a Theta Pinch Plasma. GA-4202, Gen. Dyn., June 4, 1963.

24. Bostick, Winston H.; and Wells, Daniel R.: Azimuthal Magnetic Field in the Conical Theta Pinch. Phys. Fluids, vol. 6, no. 9, Sept. 1963, pp. 1325-1331.

25. Velikhov, E. P. (J. Stuart, transl.): A Note on Plasma Rotation. J. Nucl. Energy: Pt. C, vol. 6, no. 2, Mar./Apr. 1964, pp. 203-204.

26. Haines, M. G.: Hall Rotation in Theta-Pinches. Phys. Lett., vol. 6, no. 4, Oct. 1, 1963, pp. 313-314.

27. Hintz, Eduard; and Kolb, Alan C.: Influence of Small Transverse Fields and Impurities on θ-Pinch Stability and Confinement. Phys. Fluids, vol. 8, no. 7, July 1965, pp. 1347-1355.

28. Bodin, H. A. B.; Green, T. S.; Newton, A. A.; Niblett, G. B. F.; and Reynolds, J. A.: Plasma Containment and Stability in a Megajoule Theta Pinch Experiment. Plasma Physics and Controlled Nuclear Fusion Research, Vol. I, Int. At. Energy Agency, 1966, pp. 193-221.

29. Furth, Harold P.; Killeen, John; and Rosenbluth, Marshall N.: Finite-Resistivity Instabilities of a Sheet Pinch. Phys. Fluids, vol. 6, no. 4, Apr. 1963, pp. 459-484.

30. Bodin, H. A. B.: Observations of Resistive Instabilities in a Theta Pinch. Nucl. Fusion, vol. 3, no. 3, Sept. 1963, pp. 215-217.

31. Wells, Daniel R.; and Norwood, Joseph, Jr.: Production and Propagation of Plasmoids in a Nonlinear Alfvén Wave. Phys. Fluids (Res. Notes), vol. 11, no. 7, July 1968, pp. 1582-1584.

32. Wells, Daniel R.: Observation of Plasma Vortex Rings. Phys. Fluids (Res. Notes), vol. 5, no. 8, Aug. 1962, pp. 1016-1018.

33. Wells, Daniel R.: Injection and Trapping of Plasma Vortex Structures. Phys. Fluids, vol. 9, no. 5, May 1966, pp. 1010-1021.

34. Small, R. L.; Valsamakis, E. A.; and Bostick, W. H.: Probe Measurements of Plasma Injected Into a B_z Guide Field From a Conical Theta-Pinch Accelerator. Paper No. 66-155, Amer. Inst. Aeronaut. Astronaut., Mar. 1966.

35. Jones, William B.; and Miller, R. D.: Generation of Plasmoids and Motion of the Plasmoids in a Magnetic Field With Mirrors. Bull. Amer. Phys. Soc., ser. II, vol. 11, no. 4, June 1966, p. 587.

36. Jones, W. B.; and Miller, R. D.: Generation and Motion of Plasmoids in a Magnetic Field With Mirrors. Rep. No. 67-C-178, Res. Develop. Center, Gen. Elec. Co., May 1967.

37. Niblett, G. B. F.; and Green, T. S.: Radial Hydromagnetic Oscillations. Proc. Phys. Soc. (London), vol. 74, pt. 6, no. 480, Dec. 1, 1959, pp. 737-743.

38. Glasstone, Samuel; and Lovberg, Ralph H.: Controlled Thermonuclear Reactions. D. Van Nostrand Co., Inc., c.1960.

39. Keilhacker, M.: Diffusion of Trapped Reversed Magnetic Field in a Theta Pinch in the Presence of a Probe. Nucl. Fusion, vol. 4, no. 4, Dec. 1964, pp. 287-295.

40. Eberhagen, A.; and Glaser, H.: Studies on Macroinstabilities in a Theta Pinch With Antiparallel Magnetic Field. Nucl. Fusion, vol. 4, no. 4, Dec. 1964, pp. 296-299.

41. Clark, G. L.; and Wuerker, R. F.: Plasmoid Dipole Rotation in a Theta Pinch. Phys. Fluids, vol. 5, no. 12, Dec. 1962, pp. 1503-1506.

42. Bartoli, C.; and Green, T. S.: Flip Instability of Plasma in the Theta Pinch. Nucl. Fusion, vol. 3, no. 2, June 1963, pp. 84-88.

43. Kvartskhava, I. F.; Kervalidze, K. N.; Gvaladze, Yu. S.; and Kapanadze, B. N.: Some New Data on Self-Compressed Discharges. Nucl. Fusion, 1962 Suppl. – pt. 2, pp. 533-542.

44. Kvartskhava, I. F.; Kervalidze, K. N.; Gvaladze, Yu. S.; and Zukakishvili, G. G.: Space-Periodic Plasma Structures Appearing in Fast Heavy-Current Discharges. Nucl. Fusion, vol. 5, no. 3, Sept. 1965, pp. 181-191.

45. Mather, J. W.: Diagnostics of the Confinement and Heating of a Plasma by a Rising Axial Magnetic Field (Orthogonal Pinch). Nucl. Fusion, vol. 1, no. 4, Dec. 1961, pp. 233-256.

46. Andelfinger, C.; Decker, G.; Fünfer, E.; Heiss, A.; Keilhacker, M.; Sommer, J.; and Ulrich, M.: Isar I – A Fast Megajoule Theta-Pinch Experiment With Extremely High Compression Fields. Plasma Physics and Controlled Nuclear Fusion Research, Vol. I, Int. At. Energy Agency, 1966, pp. 249-260.

47. Oertel, G. K.; and Williams, M. D.: Optical Measurement of Switch Jitter. Rev. Sci. Instrum., vol. 36, no. 5, May 1965, pp. 672-673.

48. Moon, Parry; and Spencer, Domina Eberle: Field Theory Handbook. Springer Verlag, (Berlin) 1961.

49. van der Laan, P. C. T.: Drift of a Plasma in a Curved Magnetic Field. J. Nucl. Energy: Pt. C, vol. 6, no. 6, Nov./Dec. 1964, pp. 559-566.

50. Miyamoto, Tetsu; Hamada, Shigeo; and Ohnishi, Haruyuki: End Stabilization Effect in the Slow Theta Pinch. J. Phys. Soc. Jap., vol. 23, Nov. 1967, pp. 1131-1137.

51. Goldman, L. M.; and Hurwitz, H., Jr.: Motion of θ-Pinch Plasma in Asymmetric Fields. Phys. Fluids (Res. Notes), vol. 8, no. 7, July 1965, pp. 1399-1400.

52. Furth, Harold P.: Pulsed Magnets. High Magnetic Fields, Henry Kolm, Benjamin Lax, Francis Bitter, and Robert Mills, eds., M.I.T. Press, c.1962, pp. 235-248.

53. Kilb, R. W.; Hurwitz, H., Jr.; and Westendorp, W. F.: Wall Stabilization Effects in Theta-Pinch Configurations. Phys. Fluids (Res. Notes), vol. 5, no. 9, Sept. 1962, pp. 1131-1133.

54. Kilb, R. W.; Hurwitz, H., Jr.; and Westendorp, W. F.: Wall Stabilization Effects in Theta-Pinch Configurations. Phys. Fluids, vol. 6, no. 9, Sept. 1963, pp. 1332-1337.

55. Griem, H. R.; Elton, R. C.; Kolb, A. C.; Lupton, W. H.; and Hintz, E.: The PHAROS Experiment for Producing High-Temperature Plasmas. Report of NRL Progress, Oct. 1963, pp. 1-7.

56. Little, E. M.; and Quinn, W. E.: Effects of Added Hexapole Magnetic Fields and Preionization in Theta Pinch Experiments. Phys. Fluids, vol. 6, no. 6, June 1963, pp. 875-883.

57. Gott, Yu. V.; Ioffe, M. S.; and Telkovskiy, V. G.: Some New Results on Plasma Confinement in Magnetic Traps. Nucl. Fusion, 1962 Suppl. – pt. 3, pp. 1045-1047.

58. Kim, Y. B.; and Platner, E. D.: Flux Concentrator for High-Intensity Pulsed Magnetic Fields. Rev. Sci. Instrum., vol. 30, no. 7, July 1959, pp. 524-533.

59. Herzog, R. F. K.; and Tischler, O.: Measurement of Inhomogeneous Magnetic Fields. Rev. Sci. Instrum., vol. 24, no. 10, Oct. 1953, pp. 1000-1001.

NASA-Langley, 1969 —— 25 L-5857

NATIONAL AERONAUTICS AND SPACE ADMINISTRATION
WASHINGTON, D. C. 20546

OFFICIAL BUSINESS

FIRST CLASS MAIL

POSTAGE AND FEES PAID
NATIONAL AERONAUTICS AND
SPACE ADMINISTRATION

POSTMASTER: If Undeliverable (Section 158 Postal Manual) Do Not Return

"The aeronautical and space activities of the United States shall be conducted so as to contribute . . . to the expansion of human knowledge of phenomena in the atmosphere and space. The Administration shall provide for the widest practicable and appropriate dissemination of information concerning its activities and the results thereof."

—NATIONAL AERONAUTICS AND SPACE ACT OF 1958

NASA SCIENTIFIC AND TECHNICAL PUBLICATIONS

TECHNICAL REPORTS: Scientific and technical information considered important, complete, and a lasting contribution to existing knowledge.

TECHNICAL NOTES: Information less broad in scope but nevertheless of importance as a contribution to existing knowledge.

TECHNICAL MEMORANDUMS: Information receiving limited distribution because of preliminary data, security classification, or other reasons.

CONTRACTOR REPORTS: Scientific and technical information generated under a NASA contract or grant and considered an important contribution to existing knowledge.

TECHNICAL TRANSLATIONS: Information published in a foreign language considered to merit NASA distribution in English.

SPECIAL PUBLICATIONS: Information derived from or of value to NASA activities. Publications include conference proceedings, monographs, data compilations, handbooks, sourcebooks, and special bibliographies.

TECHNOLOGY UTILIZATION PUBLICATIONS: Information on technology used by NASA that may be of particular interest in commercial and other non-aerospace applications. Publications include Tech Briefs, Technology Utilization Reports and Notes, and Technology Surveys.

Details on the availability of these publications may be obtained from:

SCIENTIFIC AND TECHNICAL INFORMATION DIVISION

NATIONAL AERONAUTICS AND SPACE ADMINISTRATION

Washington, D.C. 20546